EFFECTS OF HYDROSTATIC PRESSURE ON THE MECHANICAL BEHAVIOR OF BODY CENTERED CUBIC REFRACTORY METALS AND ALLOYS

(NASA Research Grant No. NsG-654)

INTERIM TECHNICAL REPORT

December 1967

prepared by

S. V. Radcliffe (Principal Investigator),

and G. Das

Submitted to:

Office of Grants and Research Contracts
Attention: Code SC
National Aeronautics and Space Administration
Washington, D. C. 20546

DEPARTMENT OF METALLURGY
CASE WESTERN RESERVE UNIVERSITY
CLEVELAND, OHIO

ABSTRACT

The study of the pressure dependence of tensile stress-strain behavior of recrystallized powder metallurgy tungsten at room temperature and constant strain rate has been extended to environmental pressures up to 11 kilobars. The discontinuous yield phenomena reported earlier occurs at all test pressures greater than some 3 kilobars; this reproducibility of a yield drop is in marked contrast to the reported tensile behavior at temperatures above the brittle-ductile transition at atmospheric pressure. The lower yield stress measured here in tension at high pressure and room temperature is found to be in approximate agreement with reported values from compression measurements at atmospheric pressure. However, the substructures developed during plastic straining at high pressure differ with respect to dislocation distribution and density from those for polycrystalline tungsten subjected to similar amounts of plastic strain at higher temperature at atmospheric pressure or single crystals at room temperature. Corresponding to the initiation of plastic yielding, the reduction in area at fracture increases progressively with pressure but with no indication of a brittle-ductile transition up to the highest pressure examined. Fracture occurs by a combination of intergranular and transgranular cleavage over the whole pressure range. The optical and electron microscopy observations of the free surface, fracture surface and interior indicate that the principal initial effect on fracture of increasing the environmental pressure is to inhibit the development of micro-cracks, but not their catastrophic propagation. At the highest pressure, 11 kilobars, cracks develop but propagate only slowly. The relevance of these various observations to current understanding of flow and fracture in tungsten is discussed.

In the study of the pressurization effects, earlier calculations have been revised to provide an improved basis for interpretation of the mechanism of pressure-induced dislocation generation. For the model system Fe-Fe_3C, the process of plastic deformation in a 1.4 vol.% Fe_3C alloy during tensile straining following the introduction of mobile dislocations by pressurization to 20 kilobars has been related to the accompanying changes in dislocation structure and compared with similar observations for unpressurized specimens in order to clarify the interpretation of the pressure effects.

CONTENTS

I. INTRODUCTION

The principal objectives of the present research program (which began 1 June 1967) are (a) to extend the earlier investigation of the pressure dependence of the flow and fracture behavior of tungsten in order to improve understanding and control of such behavior at both high pressure and under ambient conditions and (b) to examine the mechanism of pressure-induced generation of dislocations at elastic discontinuities and the relation between such dislocations and the associated changes in the early stages of plastic deformation, in particular in iron. Two graduate students have been involved in the research - Mr. Das on the tungsten studies, and Mr. Trester on iron - with Professor S. V. Radcliffe as principal investigator. During the early part of the present report period (1 June 1967 - 30 November 1967), Mr. Trester completed a Master of Science thesis based on research conducted under the NASA Grant and took up an industrial research post. Mr. Das has recently completed a Ph.D. thesis based on the tungsten research and is continuing with the program for a period on a post-doctoral appointment. A paper entitled "Effects of Hydrostatic Pressure on the Mechanical Behavior of Tungsten" by G. Das and S.V.Radcliffe was presented at the International Conference on the Strength of Metals and Alloys in Tokyo, Japan, in September 1967, and is being published in the Transactions of the Japan Institute of Metals. Both Mr. Trester and Mr. Das will present papers dealing with aspects of the research at the 1968 Annual Meeting of the Metallurgical Society of AIME in New York next February.

During the present six-month report period, the research carried out on mechanical behavior at pressure has been directed principally

to examining the mechanical behavior of recrystallized PM tungsten at pressures up to 11 kilobars, investigating the associated deformation and fracture modes by means of optical and electron microscopy techniques and comparing the behavior with that as a function of temperature at atmospheric pressure. In the case of pressurization phenomena, the pressure-induced stress field at an elastic discontinuity has been re-analyzed to provide a more accurate quantitative basis for a mechanism of dislocation generation and, for the model system Fe-Fe_3C, the early stages of tensile plastic straining following pressurization have been investigated in an attempt to examine directly the relation between the pressure-induced dislocations and the changes in flow stress.

II. MECHANICAL BEHAVIOR OF TUNGSTEN AT HIGH PRESSURE

In the initial study[1] of the pressure dependence of the tensile-stress behavior of tungsten, it was established that up to 3 kilobars only an increase in elastic strain to fracture is observed, but that discontinuous yielding followed by plastic straining and work-hardening occur prior to fracture for both powder-metallurgy (PM) and arc-cast recrystallized tungsten. The low value of yield stress at room temperature obtained here (96,000 psi) for the PM tungsten and the fact that no pressure-induced ductile-brittle transition phenomenon was observed within the range of pressure used are in marked contrast to the results obtained in more limited studies by earlier workers.

The current study has been concerned to examine the tensile behavior of PM tungsten over a wider range of environmental pressure and its relationship to changes in dislocation substructure. Tensile tests were

carried out at room temperature and constant strain rate at pressures up to 11 kilobars. The preparation of electro-polished tensile specimens of the PM tungsten, recrystallization treatment (2200°C in vacuum for 1 hour), high pressure apparatus and operating procedures were similar to those already described[1]. The only changes concerned the tests at the higher pressures and an improvement in the high-pressure seal for introducing electrical leads into the pressure chamber.

At pressures beyond some 8 kilobars, the glass observation windows in the pressure chamber were replaced by suitable steel plungs because of possible fracture which would cause sudden release of pressure and possible damage to the cylinder, the upper plunger and the load cell. Accordingly, strain measurement at these pressures was restricted to elongation only. The improved arrangement developed for sealing electrical leads (for the measurement of the output of the load cell and the manganin pressure transducer) in the upper plunger is shown in Figure 1. The more complex design developed by Pugh and co-workers[2] and used initially here is satisfactory in operation but difficult to replace after a lead failure. The modification involves the use of a single centrally bored hole in the piston in place of the 6 holes in the earlier design. A small conical steel plug of the same material as that of the plunger and containing six longitudinal grooves on its surface is fitted with six plastic-coated copper wires (28 gage) glued in the grooves with C-2 Armstrong epoxy cement. After curing at 150°F (65.5°C) for 1 hour, the excess epoxy is carefully filed, another layer of fresh epoxy placed on the plug and the assembly inserted in the conical hole in the upper plunger. Finally, the upper plunger containing the steel plug with the electrical leads is heated at 150°F for six hours to ensure complete cure of the

epoxy. Although this thin layer of epoxy at the interface of the conical groove and the steel plug provides adequate pressure sealing up to 11 kilobars, it was found that above 8 kilobars the electrical leads inside the groove of the plug frequently broke giving an open circuit. The breakage of the electrical leads was presumably due to tensile stresses which developed due to the relative displacement between the plug and the conical wall at high pressure. By replacing the copper wire with stronger steel wires (piano wire), this tensile failure has been avoided completely.

The fractured surfaces of the tensile specimens were examined by electron fractography using a two-stage replicating technique. A dilute solution of replicating tape (cellulose acetate) in acetone was prepared and a drop spread on a piece of the tape placed on the flat smooth surface of a glass slide. An impression of the fractured surface was then made by pressing it into the drop. After the acetone evaporated, the replicating tape was pulled out gently from the surface of the specimen. The region of the tape containing the impression of the fractured surface was cut by means of a scalpel to the size of a copper microscope grid. A thin layer of carbon together with platinum for 'shadowing' was evaporated on this film and,finally, the plastic tape was dissolved from the grid by acetone vapor leaving the shadowed carbon replica of the fractured surface.

Thin foils suitable for electron transmission microscopy were prepared from the larger tensile specimens by spark-machining transverse discs approximately 0.020 in. thick and 0.125 in. diameter from the fractured specimens, followed by spark-planing to approximately 0.010 in. thick. The discs, which were of suitable size for inserting directly into the specimen holder of the electron microscope, were then thinned to foils

by electrolytic jet-machining dimples on each face followed by bath electropolishing.

The various replica and foil specimens were examined in a JEM 6A electron microscope using a goniometer stage ($\pm$ 20° tilt, 360° rotation) and operated at 100 kV. To minimize contamination problems, a 400 micron condenser aperture was used in conjunction with a useful beam current of 100 μA.

A. Plastic Yielding

The results of the measurements of the tensile stress-strain characteristics of the recrystallized PM tungsten as a function of environmental pressure at room temperature are shown in Figure 2, including the previously reported[1] results. It is seen that the discontinuous yielding which occurs at 5 kilobars is followed by both plastic straining and work-hardening before fracture and that with further increase in pressure to 8 and 11 kilobars, the yield drop persists and the strain to fracture increases progressively. The reproducibility of the curves for a given pressure is close - with the exception of one of the 8 kilobar runs in which the lower yield stress is some 4% less than for the two other tests at that pressure. (While the results for only one of the two runs made at 11 kilobars are shown in Figure 2 because of incomplete recording due to electrical faults in the instrumentation in the other run, the reductions of area at fracture were in good agreement.)

The discontinuous yield point phenomenon observed in recrystallized PM tungsten at room temperature for pressures of 5 kilobars or higher is reproducible in that every specimen tested at 5 kilobars or higher exhibited an abrupt yield drop. Thus, the observations made here

are in qualitative agreement with the prediction[3] made from the stress-dependence of dislocation velocity in tungsten. The experimental evidence on which this prediction was based is that of Schalder and Low[4] who studied the mobility of dislocations in tungsten single crystals as a function of applied stress at 77°K and 298°K by the etch pit technique. The relationship between the experimentally observed velocity and the applied stress causing motion of the dislocations was found to conform to $\bar{V} = \left(\frac{\tau}{\tau_o}\right)^m$, where $\bar{V}$ is the average velocity, τ the applied shear stress and τ_o the stress corresponding to unit velocity and m an empirical parameter describing the stress dependence [5]. The measured values of m are 5.0 and 14.0 at 298°K and 77°K respectively. According to dislocation dynamics treatments of yielding[6,7], materials with low values of m ($\lesssim 20$) should exhibit a large abrupt yield drop when the initial density of mobile dislocations is small (10^3 - 10^4 cm^{-2}). Thus, both these conditions are likely to be met in tungsten where the grown-in dislocations interact strongly with impurity atoms.

While the phenomenon of discontinuous yielding in tungsten deformed in tension under pressure was so reproducible in the present work, the observation of yield points at 200°C and ambient pressure by Wronski and Fourdeux[8] was rare. Thus, it appears that a strong temperature-dependence of dislocation mobility and associated effects may play a significant role in determining the observation of discontinuous yielding. These differences are in keeping with the observations of Schadler and Low that the resistance to dislocation movement is increased at low temperature and the number of dislocations participating in the plastic flow is higher at high temperature than that at low temperature.

The important fact which has been shown here is that reproducible

observations of discontinuous yielding in polycrystalline tungsten at room temperature can be made only by deformation under high pressure. However, in the case of single crystals, reproducible discontinuous yielding occurs for $\langle 110 \rangle$ orientations only. While the mechanism(s) of yielding of tungsten are currently uncertain, in particular as to the cause of strong dependence of yield stress for single crystals on their orientation and the influence of the sign of the applied stress[9], a jog-controlled mechanism has been proposed by Rose et al[10] to account for the orientation dependence of higher macroscopic yield stress for this orientation. A jog-controlled mechanism was proposed also by Hanafee and Radcliffe[11] to explain their experimentally observed decrease in screw dislocation velocity in lithium fluoride as a function of pressure. The observed variation of lower yield stress of the PM tungsten with increasing test pressure (Fig.3) which exhibits a slight upward trend is in qualitative agreement with the proposal of Rose et al if the screw dislocation velocity in tungsten is jog-controlled - since the pressure effect should then be small but positive in keeping with the low activation volume. Since the measurements on the yield behavior were limited, the nature of the pressure dependence of yield stress could not be studied extensively. Accordingly, the data is represented here as lying within $\pm$ 5000 psi of a mean constant value of 96,000 psi.

The temperature dependence of the yield stress in tension cannot be measured in recrystallized PM tungsten below some 150°C at atmospheric pressure due to the onset of brittle fracture, but measurements have been reported for the compression yield stress down to -196°C. The various yield stress values which have been published[12-18] are plotted in

Figure 4. The smooth curve represents the mean of the scatter band (omitted for clarity) which encompasses the data points and it is seen that the temperature dependence appears continuous for both tension and compression yield data. The average tensile yield stress for 96,000 psi obtained at high pressure and 25°C is also plotted on this figure and lies on the lower edge of the scatter band (which ranges from 96,000 to 145,000 at 25°C with a mean of 120,000 psi). If the possible pressure dependence of the yield stress discussed above is assumed, the corresponding extrapolation to room pressure gives a value of some 83,000 psi. However, although both these values of the tensile yield stress obtained from the high pressure results are lower than those expected from the curve in Figure 4, the scatter in the previously published data is unfortunately too large to conclude that there is a difference between the yield stress in tension and compression at room temperature.

B. Dislocation Substructure

The dislocation substructure observed by thin foil electron microscopy in the series of PM tungsten specimens strained to fracture showed a discontinuous change in dislocation density and distribution with increasing pressure. The structure of the as-recrystallized tungsten exhibited only large grains separated by high-angle boundaries and containing the low density of dislocations typical of a well annealed metal. No impurity particles were found either in the grains or at the boundaries, but voids of the type discussed earlier were present. Little change occurred in this structure after fracture at atmospheric pressure and 3 kilobars with the exception of isolated dislocations which appeared at boundaries more frequently at the higher pressure. Also at 3 kilobars,

the development of internal elastic strains was evidenced by the presence of multiple diffraction contours. In contrast, the development of 2% plastic strain before fracture at 5 kilobars (see Fig. 5) resulted in both increased numbers of dislocations at boundaries and a high dislocation density within the grains, as illustrated in Fig. 5a. The dislocation arrays exhibit the dipoles, jogs and associated small loops characteristic of plastic deformation in the bcc transition metals. The nature of the dislocations at the grain boundaries is shown by the dark field micrograph in Fig. 5b. The further strain, 4% at 8 kilobars, and 8% at 11 kilobars caused a considerable increase in the density of dislocations within the grains and the development of tangles - Figures 6, 7. No twinning was observed to occur at any of the pressures investigated.

Occasional examples of grain boundary separation were seen in the foils from the 11 kilobar specimens and in one instance an associated transgranular cleavage crack penetrating partially across its grain was observed (Fig. 8). The overall length of the crack lies in a single direction, but the detailed path is made up of short zig-zag segments parallel to the two directions of straight dislocation segments visible in the foil. Although the thickness of this particular foil precluded diffraction analysis of the relevant crystallographic directions, this observation has been interpreted as direct evidence of the influence of the presence of the deformation substructure in impeding the propagation of transgranular cleavage.

The substructure developed on plastic straining at high pressure differs from that reported[8] for recrystallized polycrystalline tungsten deformed similar amounts at atmospheric pressure and 200°C, i.e. in

the region of the transition temperature, with respect to the density and distribution of dislocations. The density is seen to be comparable after deformation at room temperature and high pressure with that for 200°C and atmospheric pressure. However, the "band structure" of alternating light and dark contrast (long parallel cells separated by dislocation walls) observed by Wronski and Fourdeux to be already well developed by 7% strain does not occur. In this respect and in general appearance, the dislocation structure resembles more closely that observed recently[19] in [010] single crystals of high purity tungsten deformed in tension under ambient conditions. The density is considerably higher in the single crystal (approximately 10 times) than that observed here in the polycrystalline PM tungsten for similar values of strain - see Figure 9. The observed higher density in single crystals might arise from orientation effects since the reported[19] measurement of dislocation density as a function of strain was made on crystals oriented ((001) [010]) such that plastic flow occurs at stresses considerably below the value of macroscopic yield stress. As only ⟨110⟩ orientations are known to exhibit discontinuous yielding similar to that observed in PM tungsten here it seems possible that (001) [010] oriented crystals might contain a higher density of dislocations for comparable strain.

C. Fracture

Corresponding to the initiation of plastic yielding, the reduction of area at fracture increases with pressure above 3 kilobars. However, as shown in Figure 10, there is no indication of a transition from brittle to ductile behavior over the pressure range investigated. Also shown in Figure 10 are earlier data reported[20 - 24] for the ductility of 'tungsten'

as a function of pressure. The ductile-brittle transition indicated by these various data in the pressure range from 7 to 9 kilobars suggest that, in an analogous manner to the ductile-brittle transition temperature for tungsten, the transition pressure is higher for recrystallized material. The ductility results are in keeping with the deduction already made from the much lower yield stress values noted in the present work that the 'tungsten' used in earlier studies was not in the recrystallized condition. Examination of the pre-polished surfaces of the fractured tensile specimens by optical microscopy and of the fracture surfaces by electron fractography established that the fractures occurred by a mixture of transgranular and intergranular cleavage over the complete range of pressure. The characteristic appearance of the fracture surface is shown in Figure 11. For the specimens tested at all pressures up to 8 kilobars no evidence of cracking was found on the pre-polished surfaces except for rare example of grain boundary and transgranular cracks at the edge of the fracture surface. In contrast, the specimens fractured at 11 kilobars (8% elongation) - see Figure 12 - exhibited grain boundary cracks, occasionally with an associated transgranular crack, along the complete gage length. Most of the intergranular cracks were transverse to the tensile axis, but a number of instances of grain boundary separation in longitudinal and other directions were also noted. The transgranular cracks were not observed to propagate completely across the grains. In addition to the microcracks, occasional surface slip markings, usually associated with grain boundary junctions, were found. These various observations indicate that at pressures below 11 kilobars the principal effect of the imposed hydrostatic stress is to inhibit the formation of microcracks, but that once initiated - apparently by intergranular failure leading to transgranular cleavage - the initial crack

propagates catastrophically. In contrast, at 11 kilobars the increased plastic deformation leads to the extensive development of intergranular separation and some transgranular cracks. However, the internal cracks formed in this way do not immediately lead to failure i.e., their rapid propagation and/or the initiation of catastrophic transgranular cleavage is inhibited.

In view of the well established fact that in most crystalline materials some plastic flow accompanies fracture and the several fracture theories which assume plastic strain as a pre-requisite for the initiation of fracture, it is of interest to compare the yield stress observed at high pressure with the fracture stress at atmospheric pressure. In Figure 13, the reported data for the temperature dependence of the brittle fracture stress of recrystallized PM tungsten[12 - 16,20] is shown together with the yield stress curve from Figure 4 and the average yield stress observed at high pressure. At 25°C, the latter is seen to be close to the upper limit of the values of the fracture stress measured at atmospheric pressure, as also in the yield stress of 83,000 psi obtained by extrapolation from the high pressure data. Thus, these results are consistent with the initiation of fracture as a consequence of local plastic yielding at stress concentrations when the general stress level is below the macroscopic yield stress or, in the absence of stress concentrations, of general plastic yielding when that stress is reached i.e., it represents an upper limit for the fracture stress at room temperature.

The precise measurements made here of the pressure dependence of the fracture stress for well characterized recrystallized PM tungsten provides, for the first time, suitable data to permit the testing of theoretical

ideas concerning the effects of pressure on fracture in a brittle bcc transition metal. Detailed consideration is currently being given to this area and will be discussed in the next report.

III. PRESSURIZATION PHENOMENA

Early in this research[25] a calculation was made of the elastic stress field induced at a particle in a matrix subjected to external hydrostatic pressure. The progress of the research on structural and property changes arising from the introduction of new dislocations at particles in iron, tungsten and other materials by subjection to external pressure made it desirable to undertake a more detailed examination of the nature and magnitude of the induced stress field. In the following, this examination is described together with the results of the study of the relation of the substructure induced in a Fe-Fe_3C alloy by subjection to pressure to the subsequent plastic strain behavior under uni-axial tensile loading at atmospheric pressure.

A. Calculation of the Elastic Stress Distribution Around a Spherical Inclusion in an Isotropic Solid Under Hydrostatic Stress.

An inclusion in an isotropic solid represents a discrete reion where the elastic properties are different from those in the matrix. Voids and rigid inclusions are the limiting cases where the values of bulk moduli are zero and infinity. The presence of an inclusion disturbs an otherwise uniform stress in a solid; for example, Goodier[26] (1933) calculated a stress-concentration factor of approximately 3 near a spherical cavity in an isotropic solid subjected to uniform tension. In view

of the various experimental observations of pressure-induced dislocations at second-phase particles in Fe, Cr, W and Be, it is clearly important to extend these calculations to compute the stress distribution in the case of externally applied pressure.

A general solution for the stress-distribution around a spheroidal inclusion in an arbitrary uniform state of stress was obtained by Edwards[27] (1951). This solution was used by Hahn and Rosenfield[28] to calculate approximate values of the shear-stress at the matrix-inclusion interface induced by differential strains developed by particle growth, thermal expansion and external hydrostatic pressure. Except for this approximate calculation, no complete solution has been developed for the values of the stresses at the interface of the inclusion and matrix which specifically takes their differential compressibilities into consideration. Particular interest lies in the result that an externally imposed hydrostatic stress can give rise to shear stresses at the interface,since nucleation of dislocations at the inclusion-matrix interface is possible if the shear stress exceeds a critical value of approximately one tenth of the shear modulus. Under such circumstances an inclusion in the matrix could be converted by simple application of hydrostatic pressure into a source of dislocations which could strongly influence the plastic behavior of the solid. Accordingly, precise knowledge of the maximum shear stress attainable at the interface is needed to determine the possibility of dislocation nucleation under such conditions.

An attempt has been made here to calculate rigorously the maximum shear stress generated at the interface between an elastic discontinuity and its surrounding matrix for a solid subjected to external hydrostatic pressure. The calculations followed the continuum mechanics principles

outlined by Sokolnikoff[29] and assumed that the elastic properties of the matrix and the inclusion are isotropic, the inclusion is spherical with a smooth surface and the stress fields of different particles do not interact. Under these conditions, the maximum shear stress, τ_{max}, which develops at the inclusion-matrix interface is given by the following relationships for the three cases of a cavity, a rigid inclusion and an elastic inclusion:

$$\text{Cavity} \qquad \tau_{max} = \frac{3}{4} P \tag{1}$$

$$\text{Rigid inclusion} \qquad \tau_{max} = \frac{G}{K} P \tag{2}$$

$$\text{Elastic inclusion} \qquad \tau_{max} = \frac{3G}{K} P \left[\frac{K - K_i}{3K_i + 4G} \right] \tag{3}$$

where G is the shear modulus of the matrix, P is the applied hydrostatic pressure, K and K_i are the bulk moduli of the matrix and the inclusion respectively, (For details of the calculations, see Doctoral Thesis of G. Das, Case Western Reserve University, 1967) - see Figure 14.

The values of maximum shear stress for the cases of cavity, rigid inclusion and elastic inclusion with similar and dissimilar elastic constants based on the calculations used here are listed in Table I. The table also contains the value of τ_{max} for appropriate inclusions as calculated by Hahn and Rosenfield[28]. Table II contains values of maximum shear stress computed for cavities, thoria and hafnium carbide in a tungsten matrix as a function of the externally applied hydrostatic pressure. It is seen from Table II that the induced stresses are substanially less, even at 20 kilobars, than 10^{-1} G, the stress theoretically required to generate dislocations in a perfect crystal[30]. However, for a small indentor (10^{-4} cm diameter) - e.g. silicon carbide particles dropped on to a crystal surface - a contact pressure of 10^{-3}G is sufficient to "punch-in" dislocation loops. This observation can be explained only if

it is assumed that the indentors possess atomistically sharp steps. A stress concentration of $2(D/2b)^{\frac{1}{2}}$ can be achieved for a particle of diameter D and the crystal of Burger's vector[30]. For a 1 micron particle, this stress concentration factor is about 100. Thus, the stress at the edge of the indentor becomes of the order of $10^{-1}G$, as required for dislocation generation. From the calculated magnitude of shear-stresses induced by differential compression as shown in Table II, it is apparent that dislocations would be expected to be generated only if the particles are irregular in shape or exhibit very sharp steps on their surfaces which can act as stress-raisers.

Another factor which could favor generation of dislocations would be the existence of residual stresses around the interface of the inclusion and matrix. Although Goodier's[26] calculations of stress-concentrations at elastic discontinuities in solids under tensile stress indicate that the shear stress is increased locally by a factor of only approximately 3, the recent literature contains a number of observations[31,32,33] of particles under stress acting as dislocation sources. Particularly good examples of punched-in dislocations are those around FeO particles in iron deformed 2% in tension as reported by Kayano[33] who concluded that residual stresses around the inclusion induced thermally during cooling are responsible for such dislocation generation during subsequent tensile deformation. It is possible that such residual stresses could similarly assist the generation of dislocations when a matrix containing an inclusion is subjected to high hydrostatic pressure.

The stress field which arises around an inclusion during cooling due to differential contraction is analogous to that which is developed on pressure application as a result of differential compressibility.

Therefore, it is logical to assume that the nature of the thermally-induced dislocation would be similar to the pressure-induced dislocation. Although complete analysis of pressure-induced dislocations at particles has not been reported, Jones and Mitchell[34] have examined in detail how a dislocation can be nucleated by differential thermal contraction at the surface of glass spheres in silver chloride. If such a dislocation is nucleated at the surface of the glass sphere in the region of maximum shear, it can glide on the surface of a cylinder with its Burger's vector as axis. The stages of formation of a loop by pure glide are shown in Figure 15. Under the influence of shear stresses, only the edge component can glide outward away from the region of maximum shear stress and the screw components parallel to the axis of the cylinder experience tangential forces which causes them to glide in opposite directions around the surface of the glide cylinder. Because the shear stress decreases as the distance from the inclusion increases, the edge component cannot travel as far as the screw components, which are always in the region of maximum shear stress. When two ends of the original dislocation meet, a fully developed prismatic dislocation loop is formed. In addition to explaining the formation of loops by prismatic punching, this mechanism allows transport of material from the particle-matrix interface to region of lower stress in the matrix. Thus, this prismatic dislocation loop will be interstitial in nature. Although the interstitial nature of the loop was predicted by Jones and Mitchell, identification of their nature could not be made by the decoration method used to reveal dislocations. However, by transmission electron microscopy, Lawley and Meakin[35] proved that the dislocations originating at particles precipitated in molybdenum during cooling (due to differential contraction) are interstitial in

nature. Thus, based on these various observations of thermal dislocations and in view of the similarity of the stress field generated in both the pressure and thermal cases, the pressure induced dislocation loops would also be expected to be interstitial in nature. The observations made here on the nature of pressure-induced loops formed from particles in an iron matrix are in keeping with this interpretation.

B. Relation of Pressure-induced Sub-structure to Plastic Strain Effects.

On the basis of the observations of the micro and macroyield behavior of the pressurized iron-carbon alloys and the corresponding pressure-induced substructural changes discussed in the earlier reports[1], the principal features of relationships between the induced defect structure and the mechanical behavior were deduced. In an attempt to assist in developing a more quantitative and direct interpretation of the relationships, a thin-foil electron microscopy study has been made of the changes in substructure as a function of tensile strain in a Fe-0.09 wt.% C (1.4 vol.% Fe_3C) alloy which was previously pressurized.

After subjection of annealed specimens to a hydrostatic pressure of 20 kilobars, using the procedures described previously[1], the following tensile straining procedures were carried out. One specimen was stressed to 13.0×10^3 psi (a stress similar to the σ_A value of 12.2×10^3 psi determined in an identical specimen during the cyclic loading study of microstrain phenomena) and after reaching this load, the tensile stress was removed. The same procedure was followed with identically pressurized specimens to prestrains of 1.0 and 5.3%. In addition, an annealed specimen was prestrained to 6.5% as a reference. The various procedures are illustrated in Figure 16. Thin foils were prepared from discs spark-sliced from gage length of the tensile specimens and examined by transmission

electron microscopy. The features observed will be brought into the following discussion of the yield behavior at appropriate points.

The stress-strain curves of pressurized alloys can be compared with those of as-annealed alloys in terms of the current theories of the yielding of iron discussed earlier[1]. Initially, the curves for both conditions demonstrate the same elastic relationship upon loading, as depicted by the schematic representation in Figure 17. At some point, a or a', (which decreases in value with increase in the magnitude of the maximum pressure applied prior to the test) the strain is observed to deviate from its linear ("elastic") relationship with stress and a high rate of work-hardening is exhibited. Beyond a deviation of 10^{-5} to 10^{-4} in/in from the elastic relationship, the initially high rate of hardening gradually decreases, demonstrating the onset of macroyielding. Figure 18 illustrates the dislocation substructure of the pressurized 1.4 vol.% Fe_3C alloy after tensile prestraining to σ_A. In interpreting these it is helpful here to recall[1] that the initial pressure-induced substructure in this alloy exhibits a characteristic increase in dislocation arrays surrounding second-phase particles. To be noted in the prestrained specimens compared to the as-pressurized condition is the non-uniform increase in clusters of tangled dislocations within the grains and the relatively larger density of dislocation clusters in the vicinity of carbide particles. As expected, a definite dislocation cell structure is not developed at this strain and many regions adjacent to the clusters are often relatively sparse in dislocation content. However, the observations confirm the movement and multiplication of pressurized dislocations in the microyield region.

The unique event which follows this initial region of plastic flow

is manifested by a sharp macroyield point in the annealed material in contrast to a gradual yield drop in the alloys subjected to pressure. The lower yield stress decreases progressively with the amount of prior pressurization and at a particular value of the applied pressure, peculiar to each alloy and its microstructural characteristics, the yield drop disappears. Another important characteristic of the pressurized alloys is the low stress at which the transition occurs from microyield to the succeeding macroyield region, i.e. the stress at which the barrier presented by grain interfaces to the contained dislocations is transcended and some form of rapid yielding process occurs, thereby accommodating the applied strain rate. Since both pressurized and unpressurized specimens received the same thermal treatment, the grain boundary strength (as affected, for example, by segregation of impurity elements, particularly interstitials) and the distribution and morphology of second-phase particles should be similar for both. Accordingly, it can be deduced that the stress concentrations are greater at the grain interfaces in the pressurized material as a result of the denser pileup of slip bands formed by the many pressure-induced dislocations in addition to those generated by multiplication processes during loading. For this reason, along with the tendency for strain to be more uniformly distributed along the gage length, (in marked contrast to the annealed specimens which yield by Luders' band propagation through relatively unyielded grains) the pressurized specimens can undergo significant macroyielding at a lower measured tensile stress than the unpressurized material. The gradual disappearance of the yield drop with increasing pressurization is qualitatively consistent with yield theories based on the rapid multiplication of dislocations and stress dependence of dislocation velocity[36].

Once macroyielding is initiated, the stress-strain relationship in the pressurized alloys is characterized by a relatively short Luder's plateau or, for some compositions, a gradually increasing slope which eventually becomes equal to that of the work-hardening curve for the annealed (un-pressurized) material. In the cases where a Luders strain is exhibited, the length of the plateau decreases with increasing applied pressure, as shown in the schematic curves. In all the alloys examined, later stages of work-hardening after pressurization eventually equal that characteristic of the annealed material. It is possible that in the materials subjected to pressures high enough to eliminate a yield drop, the rapid decrease in the slope of the stress-strain curve to the $d\sigma/d\varepsilon = 0$ portion of macroyielding prior to work-hardening is not due to a Luders band phenomenon but instead represents a region where extensive dislocation multiplication is occurring throughout the gage length. This interpretation would account for the decrease observed in the strain at the beginning of work-hardening with increase in the magnitude of the pressure applied. The comparative electron microscopy structures of the 1.4 vol.% Fe_3C alloy annealed and prestrained 6.5% (Fig. 19) and pressurized and prestrained 5.3% (Fig. 20), exhibit little obvious difference in substructure, except for a slightly greater density of dislocations in the former. Compared with the substructural observations in the specimen of the same material prestrained to only σ_A, the dislocations have increased substantially in number and distribution, and dislocation-free regions are considerably smaller in area. Prior subgrain boundaries have dissociated extensively and a cell structure has developed from the earlier clusters. Regions near grain boundaries and second-phase particles exhibit the highest density of dislocations. The likeness between the substructures is consistent with

the similarity in stress-strain behavior in both types of specimen which develops after their dissimilar earlier stages of micro- and macro-yield behavior.

In conclusion, the direct observations of the pressure-induced substructure, the nature of dislocation structure in material tensile strained after pressure-cycling and the corresponding flow stress changes as a function of pressure have provided a qualitative basis for understanding the effects of pressure on yield behavior in a series of Fe-Fe_3C alloys for a variety of different structural conditions. However, the complex and interacting roles played by microstructural components, initial substructure, and composition of a given material during both pressure cycling and tensile yielding make it difficult at the present time to develop a more quantitative model which can account for the details of the yield behavior in the pressure-cycled Fe-Fe_3C alloys.

IV. FUTURE WORK

During the next six-month period, the study of the flow and fracture behavior of arc-melted tungsten will be extended to higher pressures. On the basis of the resulting experimental data for yield and fracture stresses, together with those already determined for powder-metallurgy tungsten, attempts will be made to evaluate recent theoretical calculations of the effects of pressure on these parameters. The role of impurities, grain size and structural imperfections in determining the flow stress will also be examined. The significance of the results for the understanding of the mechanical behavior of tungsten at atmospheric pressure will be considered. In the case of pressurization effects, an alternate model system consisting of copper containing helium-filled voids will be analyzed to test the validity of the arguments presented previously on the basis of calculations of the pressure-induced stress fields at a discontinuity in a matrix.

V. REFERENCES

1. S. V. Radcliffe, G. Das, and P. Trester: Interim Technical Rept.No.6 (NASA Grant No. NsG-654) June 1967, Case Institute of Technology.

2. (a) H.Ll.D. Pugh and D. Green: "Behavior of Metals Under High Hydrostatic Pressure", MERL Plasticity Rept. No. 128, National Engineering Laboratory, 1956.

   (b) H. Ll.D. Pugh, J. Lees, K. Ashcraft and D. Gunn: Engineer (G.D.), 212 (1961) 258.

3. R. I. Jaffee and G. T. Hahn: The Relation Between the Structure and Mechanical Properties of Metals, H.M.S.O. 2 (1963) 708.

4. H. W. Schadler and J. R. Low: "Low-Temperature Brittleness of Refractory Metals", O.N.R. Report on Contract Nonr-2614(00),April 1962.

5. W. G. Johnston and J. J. Gilman: J.Appl. Phys.,30 (1959), 129.

6. W. G. Johnston: J. Appl. Phys.,33 (1962), 2716.

7. G. T. Hahn: Acta Met., 10 (1962), 727.

8. A. Wronski and A. Fourdeux: Phil. Mag.,10 (1964) 969.

9. D. Hull, J. F. Bryan and F. W. Noble: Can. J. Phys.,45 (1957), 1091.

10. R. M. Rose, D. P. Ferriss and J. Wulff, Trans.AIME,224 (1962), 981.

11. J. Hanafee and S. V. Radcliffe: J. Appl. Phys, 38, (1967), 4284.

12. A. Wronski and A. Fourdeux: J. Less-Common Metals,8 (1965), 149.

13. J. H. Bechtold and P. G. Shewmon: Trans. ASM,46 (1954), 397.

14. J. W. Pugh: Proc: ASTM,57 (1957), 906.

15. C. R. McKinsey, A. L. Mincher, W. F. Sheeley and J. L. Wilson: ASD TR 61-3, July 1961.

16. B. C. Allen, D. J. Maykuth and R. I. Jaffee: J.Inst. Metals,90 (1961),120.

17. R. H. Schnitzel: J. Less-Common Metals, 8 (1965), 81.

18. W. R. Witzke, E. C. Sutherland and G. K. Watson: Tech. Rept. TND-1707, National Aeronautics and Space Administration, 1963.

19. B. Warlimont-Meier, P. Beardmore and D. Hull: Acta Met.,15 (1967), 1399.

20. P. W. Bridgman: J. Appl. Phys., 24 (1963), 560.

21. L. D. Livshitz, Y. N. Ryabinin and B. I. Beresnev: Soviet Phys. - Tech. Phys., 10 (1965), 278.

REFERENCES (Continued)

22. A. Bobrowsky: Paper 64-WA/PT-29, Symposium of High Pressure Technology, Am. Soc. Mech. Eng., New York (1965).

23. T. E. Davidson, J. C. Uy and A. P. Less: Acta Met., 14 (1966), 937.

24. H. Ll. D. Pugh: Bulleid Memorial Lectures, Nottingham University Press (1965).

25. S. V. Radcliffe and G. Das: Interim Technical Report (NASA Grant NsG-654) June 1965, Case Institute of Technology.

26. J. N. Goodier, Trans. ASME 55 (1933) APM-55-7-39.

27. R. H. Edwards: J. Appl. Mech. 18 (1951) 19.

28. G. T. Hahn and A. R. Rosenfield: "Effects of Second Phase Particles on Ductility", Battelle Memorial Institute, Tech. Rept. AFML-TR-65-309 (Sept. 1964).

29. I. Sokolnikoff: Mathematical Theory of Elasticity, McGraw-Hill Book Co. Inc., New York, 1956, 344.

30. J. Friedel: G. Thomas and J. Washburn, Eds., Electron Microscopy and Strength of Crystals (Interscience, N. Y.), 1963, p. 605.

31. J. R. Patel, J. Appl. Phys., 33 (1962), 2223.

32. W. C. Leslie, Acta Met., 9 (1961), 1004.

33. H. Kayano, J. Japan Inst. Metals, 31 (1967), 310, 316.

34. D. A. Jones and J. W. Mitchell, Phil. Mag. 8 (1963), 1713.

35. A. Lawley and J. D. Meakin, Phil. Mag. 10 (1964), 737.

36. G. T. Hahn, Acta Met. 10 (1962), 727.

37. A. H. Cottrell: The Mechanical Properties of Matter, John Wiley and Sons, Inc. 1964.

38. Peter T. B. Shaffer: High Temperature Materials No. 1 Materials Index, Plenum Press, New York, 1964.

TABLE I

Calculated values of radial, circumferential and shear stresses developed in the matrix for the three cases of cavity, rigid and elastic inclusion upon subjection to external hydrostatic pressure.

Case	Reference	σ_r in Matrix	σ_θ in Matrix	τ_{max} (AT r=a)
I. Cavity	Present Calculation	$-P\left(1-\frac{a^3}{r^3}\right)$	$-P\left(1+\frac{a^3}{2r^3}\right)$	$\frac{3}{4}P$
II. Rigid Inclusion	Hahn and Rosenfield Eqn.			$\approx\frac{P}{3}$
	Present Calculation	$-P\left[1+\frac{2(1-2\nu)}{1+\nu}\cdot\frac{a^3}{r^3}\right]$	$-P\left[1-\frac{1-2\nu}{1+\nu}\cdot\frac{a^3}{r^3}\right]$	$\frac{G}{K}P$
III. Elastic Inclusion	Hahn and Rosenfield[28]			$\phi\frac{P}{3}\left[\frac{(K-K_i)}{K_i}\right]$
	Present Calculation	$-P\frac{3E_i(1-\nu)}{(1+\nu)E_i+2(1-2\nu_i)E}$	$-P\frac{3\nu E_i+3(1-2\nu_i)E}{(1+\nu)E_i+2(1-2\nu_i)E}$	$\frac{3G}{K}\left[\frac{K-K_i}{3K_i+4G}\right]P$

Symbols Used in Table I.

$-P$	-External hydrostatic pressure.
ν, ν_i	-Poisson's ratio of the matrix and inclusion, respectively.
G	-Shear modulus of the matrix.
a	-the radius of the inclusion.
K, K_i	-Bulk modulus of the matrix and inclusion, respectively.
$\sigma_r, \sigma_\theta, \sigma_\phi$	-Radial, circumferential and azimuthal stress, respectively.
τ_{max}	-Maximum shear stress
ϕ	-A factor ≈ 1 determined by the ratio of Young's moduli of the inclusion and matrix.
r_o	-Radius vector.
E, E_i	-Young's modulus of matrix and inclusion, respectively.

TABLE II

Calculated stress, τ_{max} at spherical cavities, rigid inclusions, and elastic inclusions, in tungsten matrix as a function of the applied hydrostatic pressure.

Matrix	Hydrostatic Pressure	τ_{max} Cavity		Rigid Inclusion		Elastic Inclusion ThO_2		Elastic Inclusion HfC	
Tungsten	10 kb	111×10^3	$\frac{G}{200}$	79×10^3	$\frac{G}{275}$	24.7×10^3	$\frac{G}{900}$	17.0×10^3	$\frac{G}{1300}$
	20 kb	222×10^3	$\frac{G}{100}$	159×10^3	$\frac{G}{137.5}$	49.4×10^3	$\frac{G}{450}$	34.0×10^3	$\frac{G}{650}$
	25 kb	278×10^3	$\frac{G}{80}$	200×10^3	$\frac{G}{110}$	61.8×10^3	$\frac{G}{360}$	42.5×10^3	$\frac{G}{520}$
	40 kb	444×10^3	$\frac{G}{50}$	318×10^3	$\frac{G}{68.8}$	98.8×10^3	$\frac{G}{225}$	68.0×10^3	$\frac{G}{325}$

Data*used in stress calculation for Tungsten:

	Tungsten	HfC	ThO_2
Shear Modulus G (Psi)	22×10^6	-	-
Youngs Modulus E (Psi)	56.5×10^6	-	-
Poisson's Ratio	0.27	-	-
Bulk Modulus, K (Psi)	40.9×10^6	30.7×10^6	25.9×10^6

*All data taken from Ref. 37 except for THO_2 and HfC (Ref. 38).

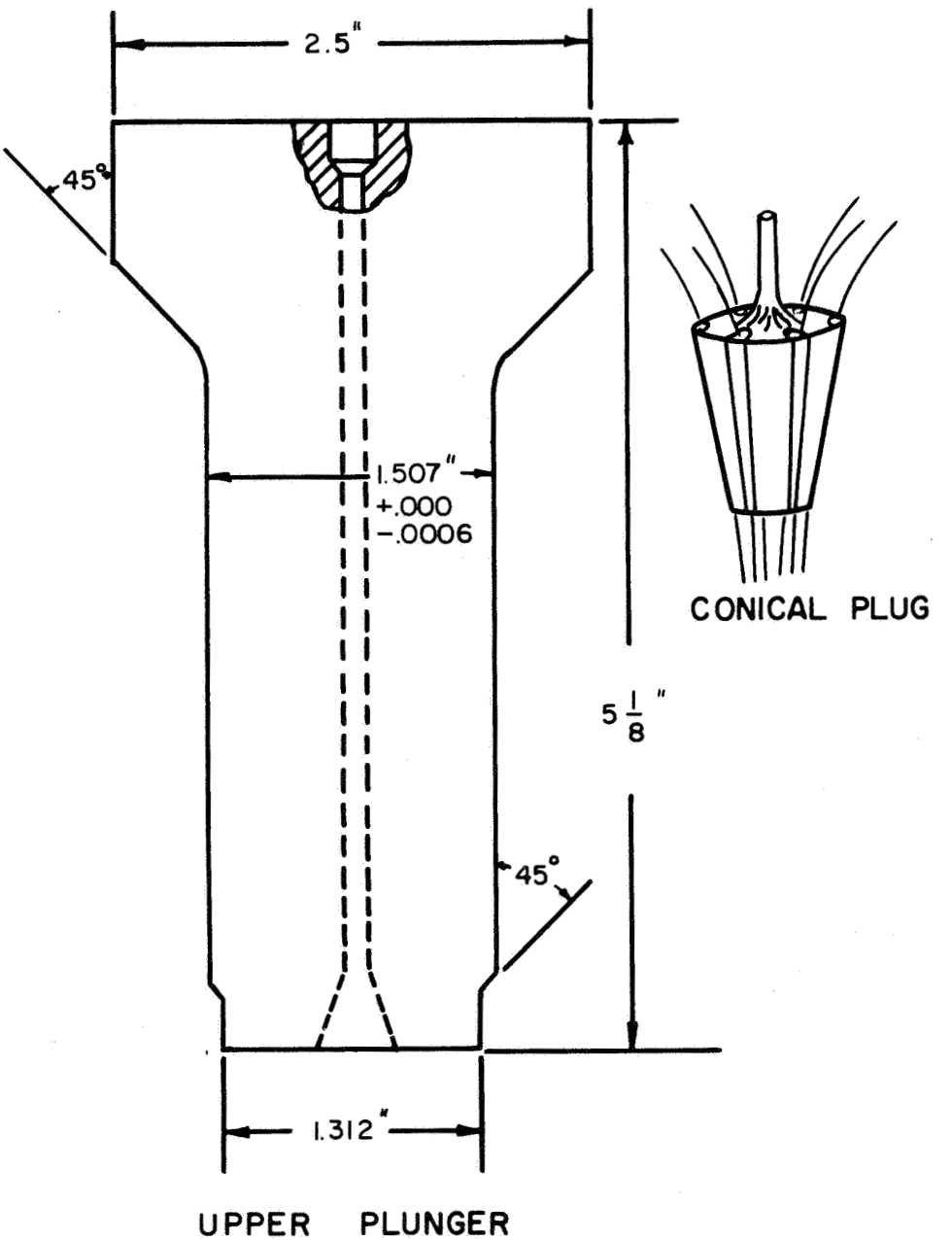

Fig. 1. Details of upper plunger of main high pressure chamber and conical plug design for pressure seal for electrical leads.

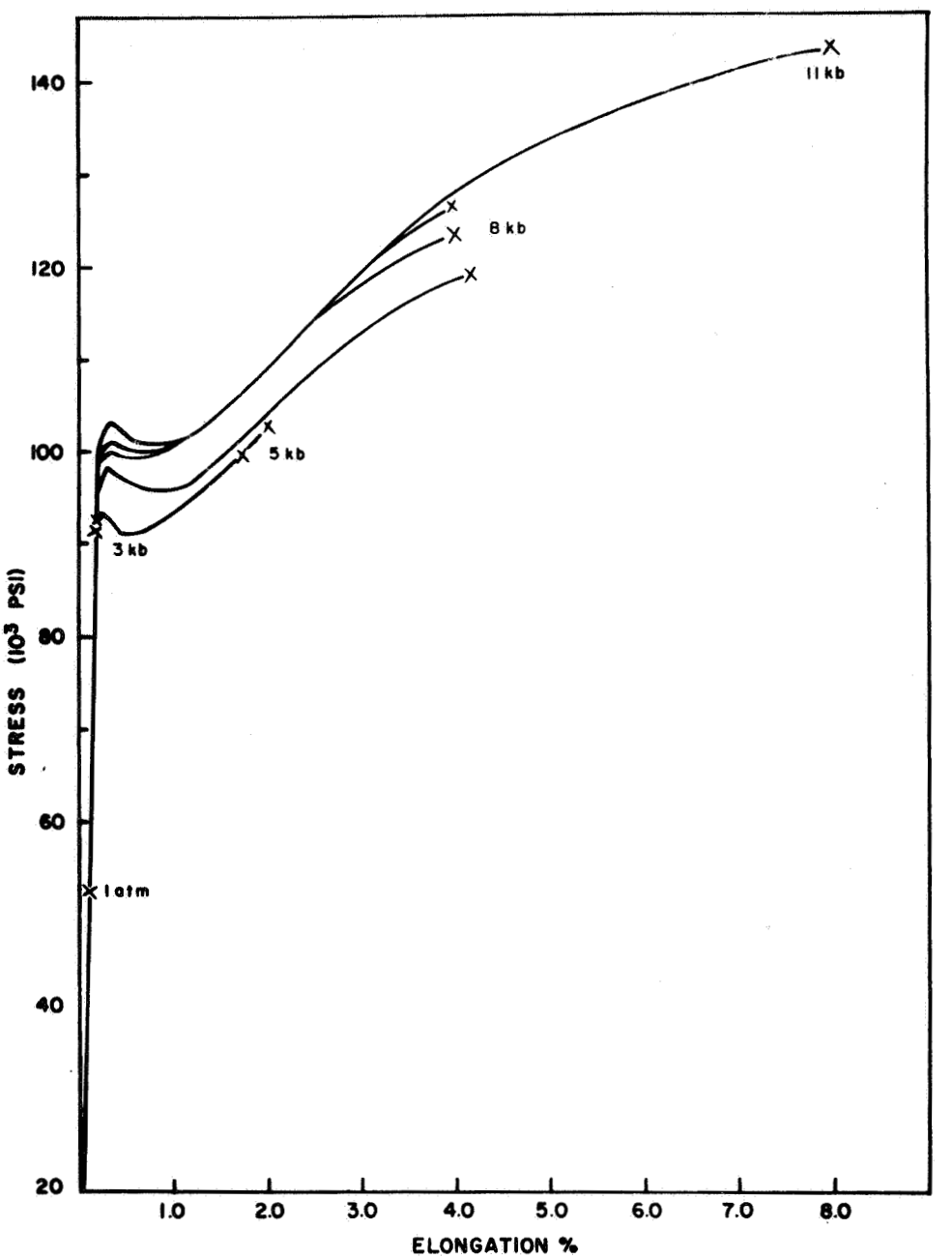

Fig. 2. Tensile stress-strain curves for recrystallized PM tungsten as a function of environmental pressure at room temperature.

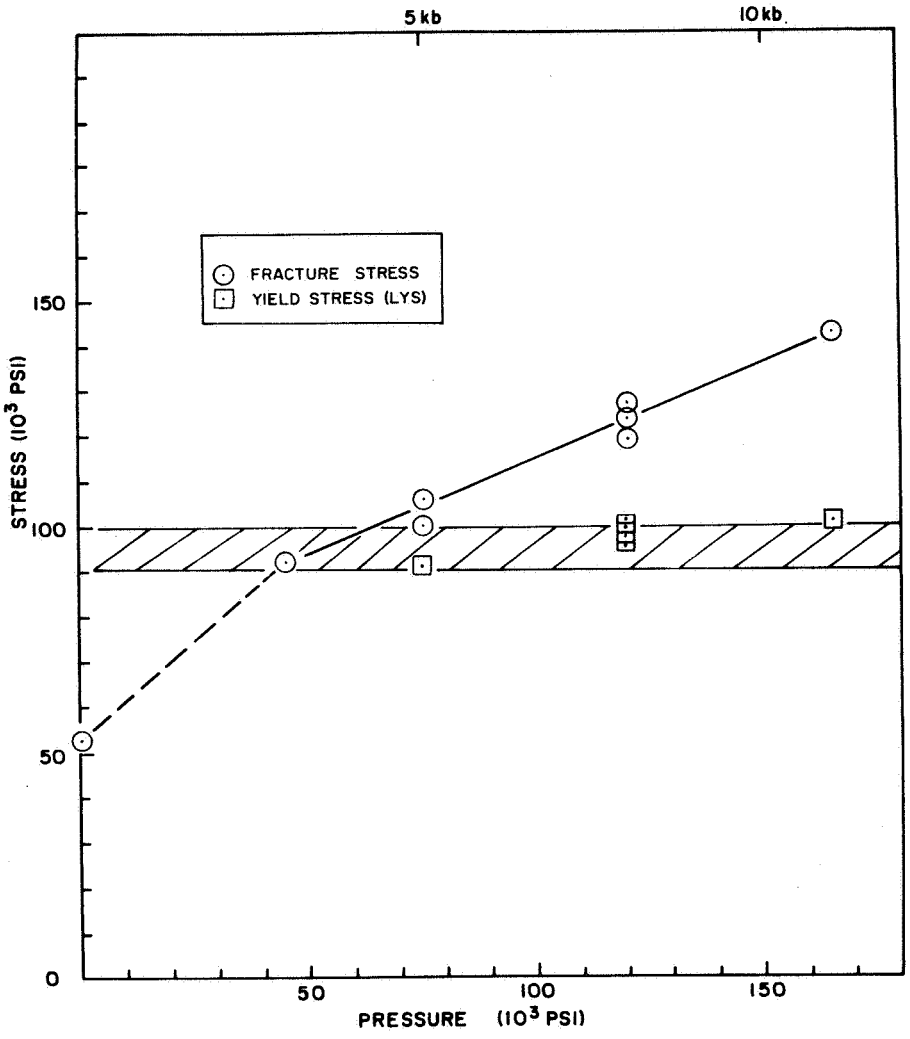

Fig. 3. Pressure dependence of yield and fracture stresses in tension of recrystallized tungsten.

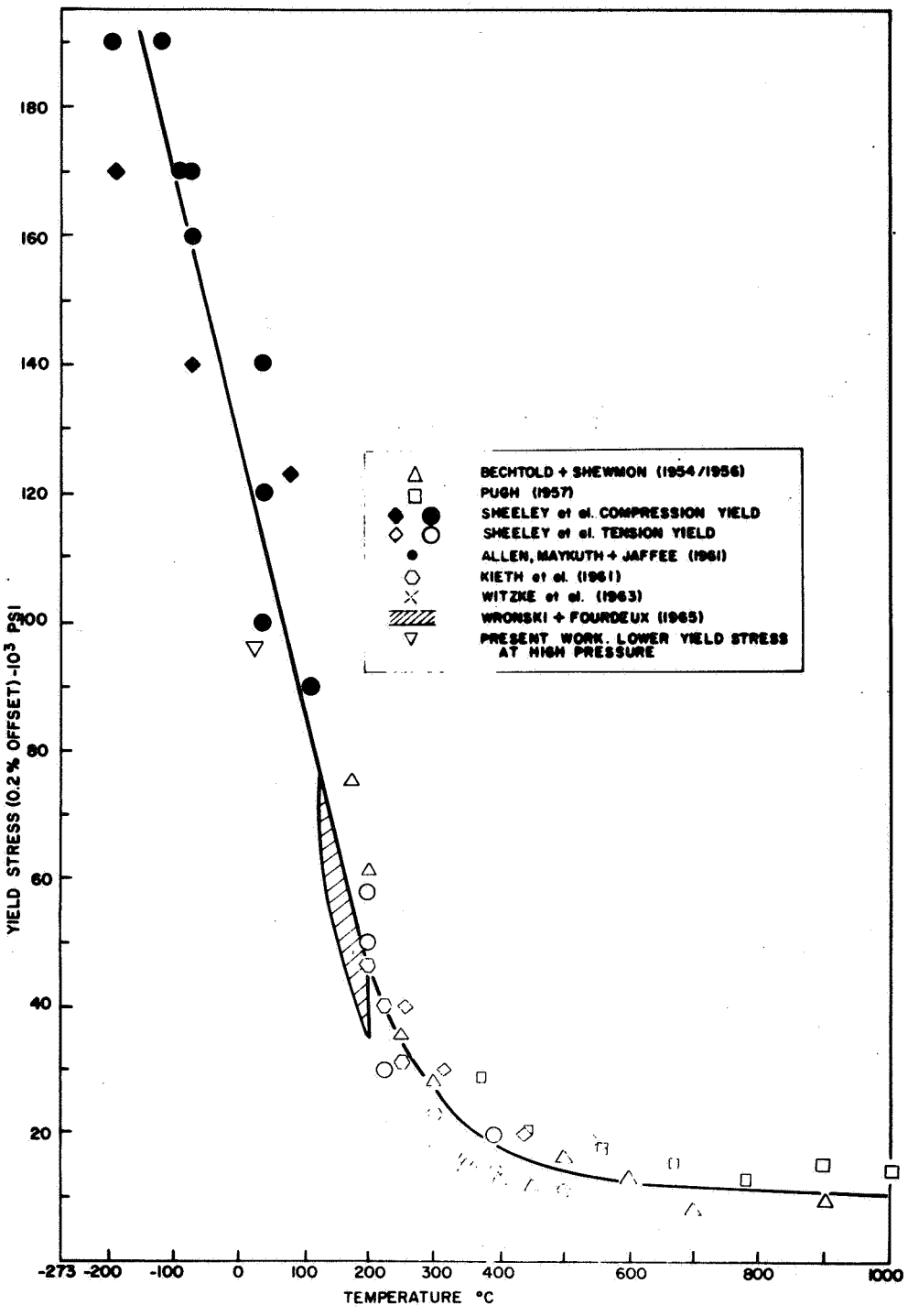

Fig. 4. Compilation of reported measurements of yield stress in tension and compression for recrystallized PM tungsten at atmospheric pressure.

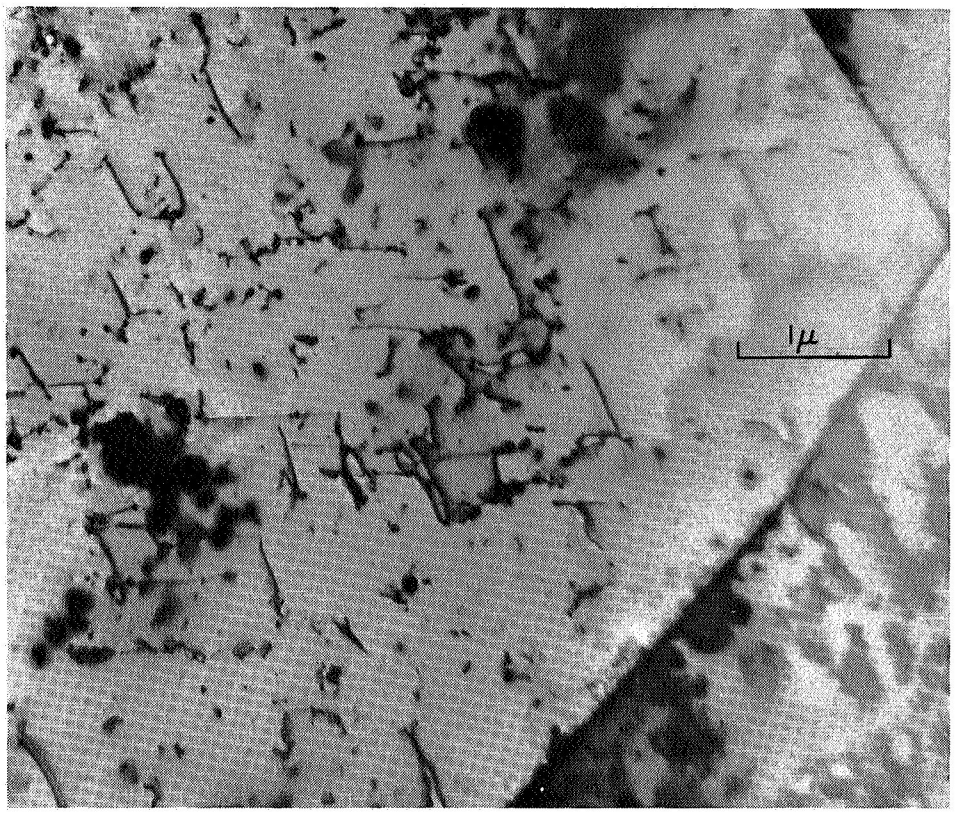

(a)

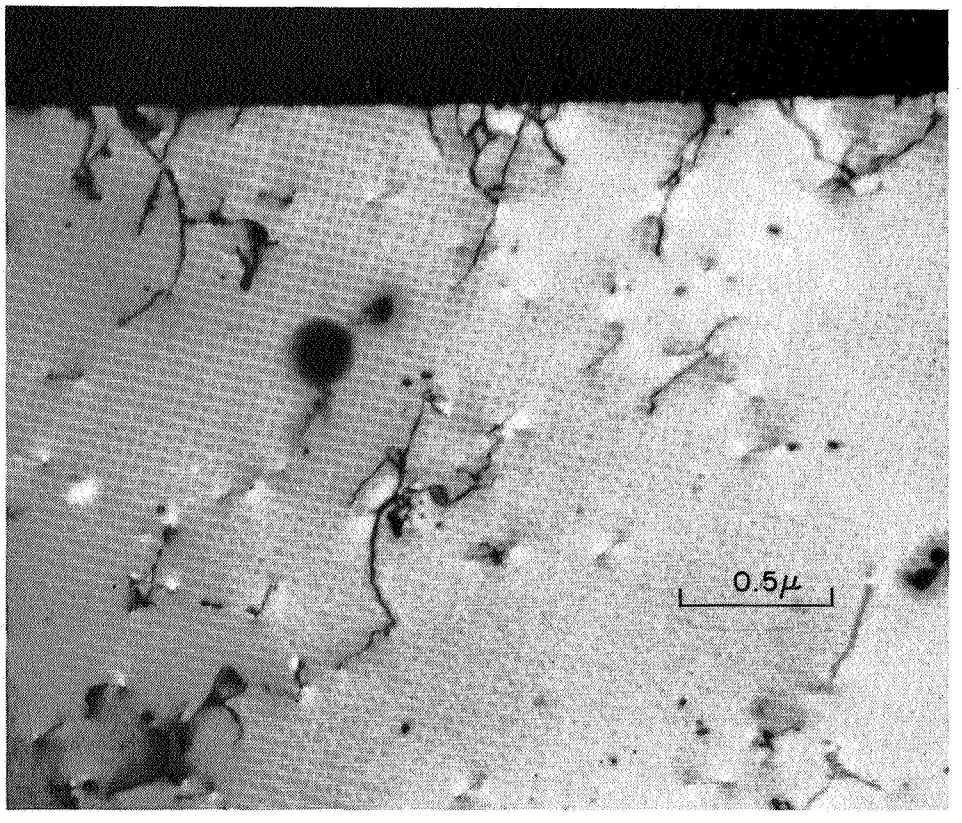

(b)

Fig. 5. Thin foil electron micrographs illustrating substructure of recrystallized PM tungsten strained to fracture at 5 kilobars and room temperature. 2% elongation.

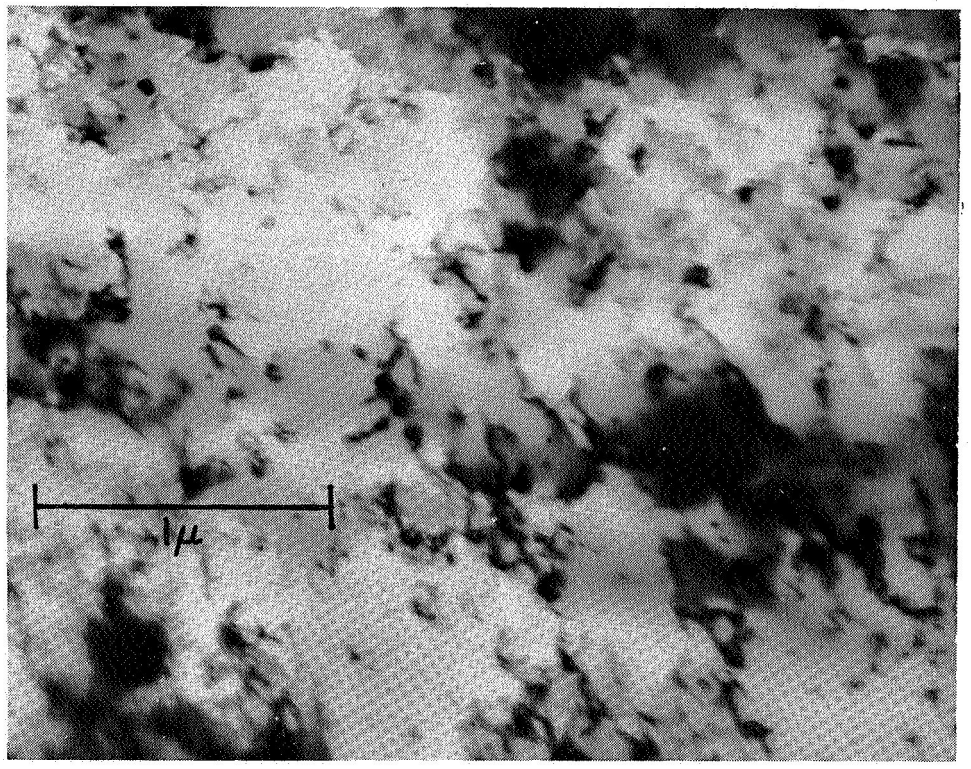

(a)

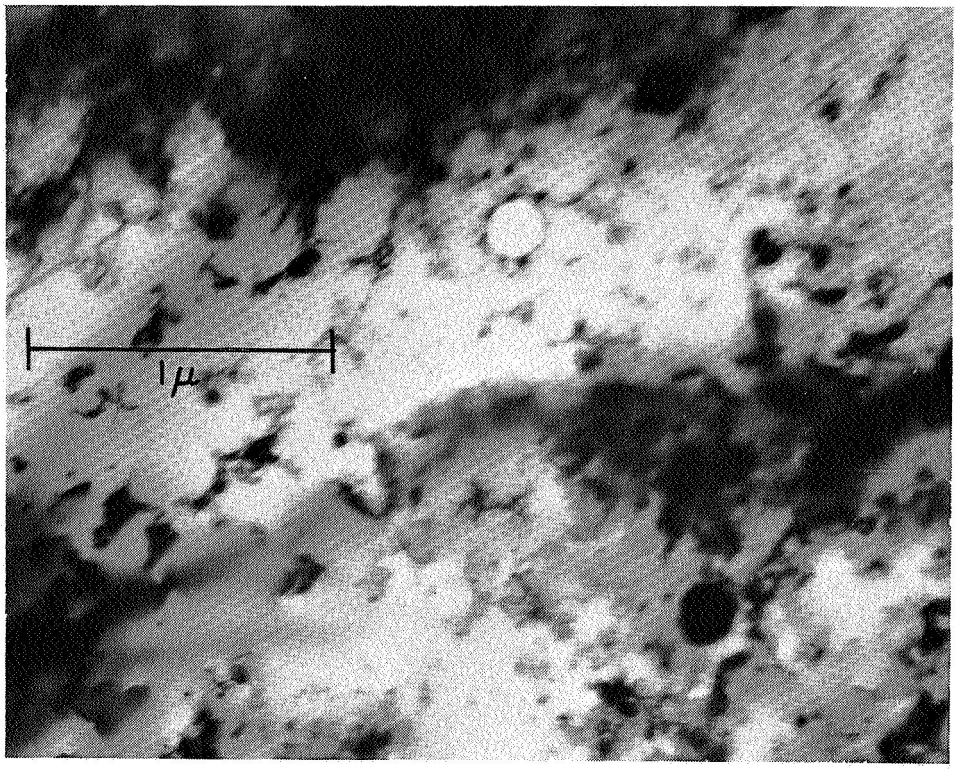

(b)

Fig. 6. Thin foil electron micrographs showing dislocation substructure of recrystallized PM tungsten strain to fracture at 8 kilobars at room temperature. 4% elongation.

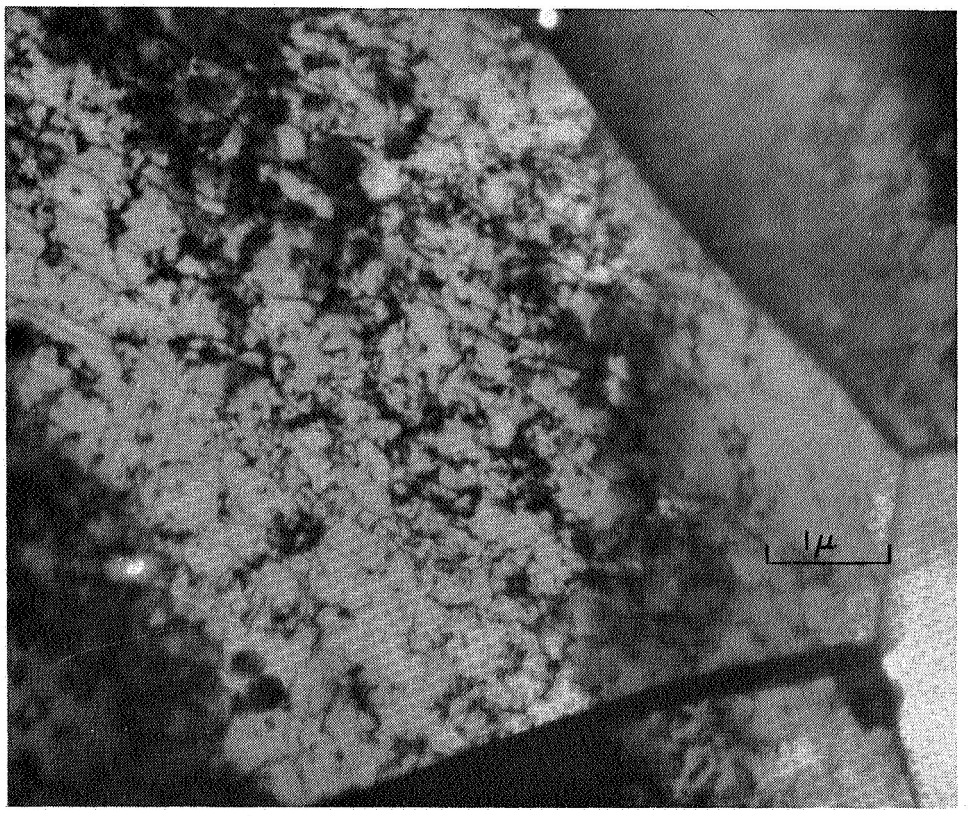

(a)

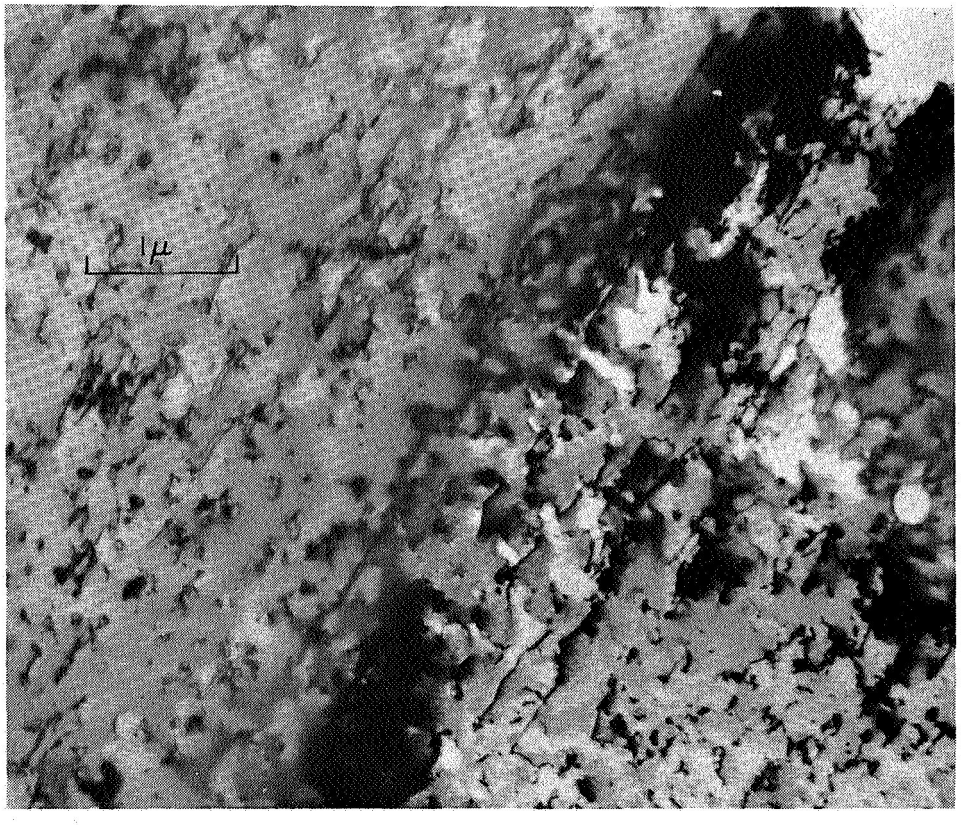

(b)

Fig. 7. Substructure of recrystallized PM tungsten strained to fracture at 11 kilobars and room temperature. 8% elongation.

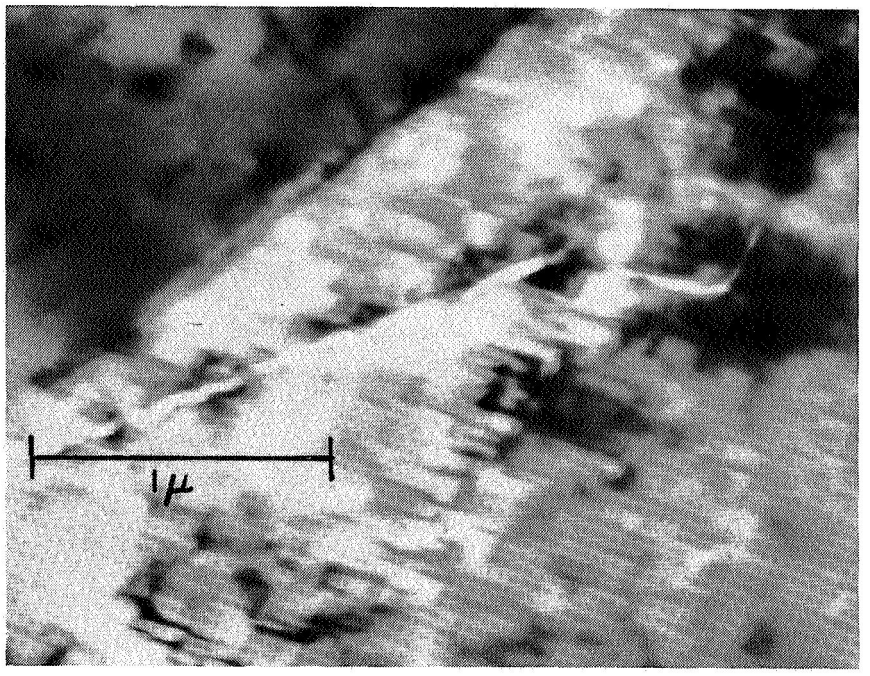

(a)

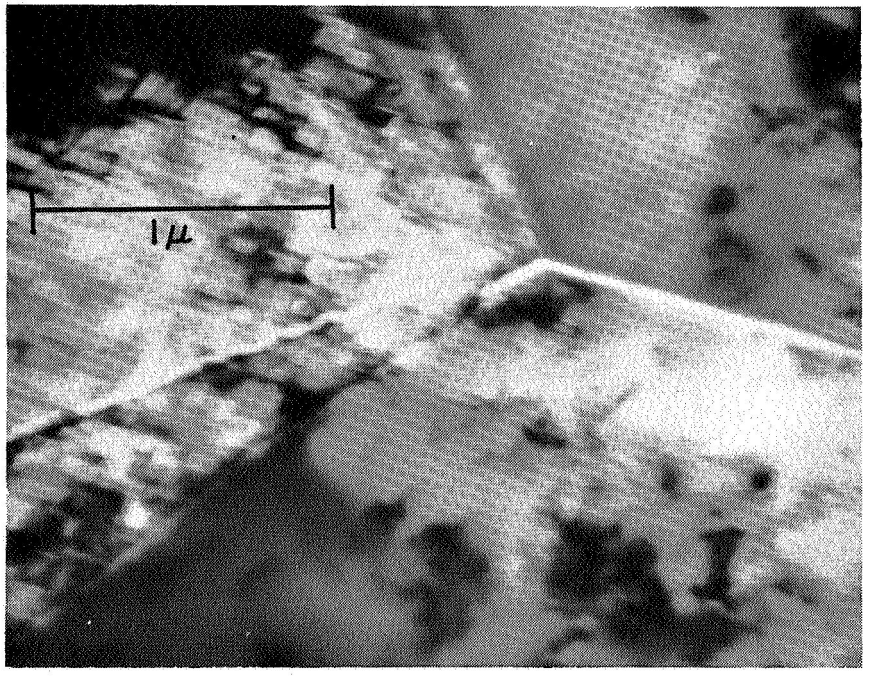

(b)

Fig. 8. Substructure of recrystallized PM tungsten strained to fracture at 11 kilobars at room temperature, showing (a) a transgranular crack with short zig-zag segments; (b) an intergranular crack.

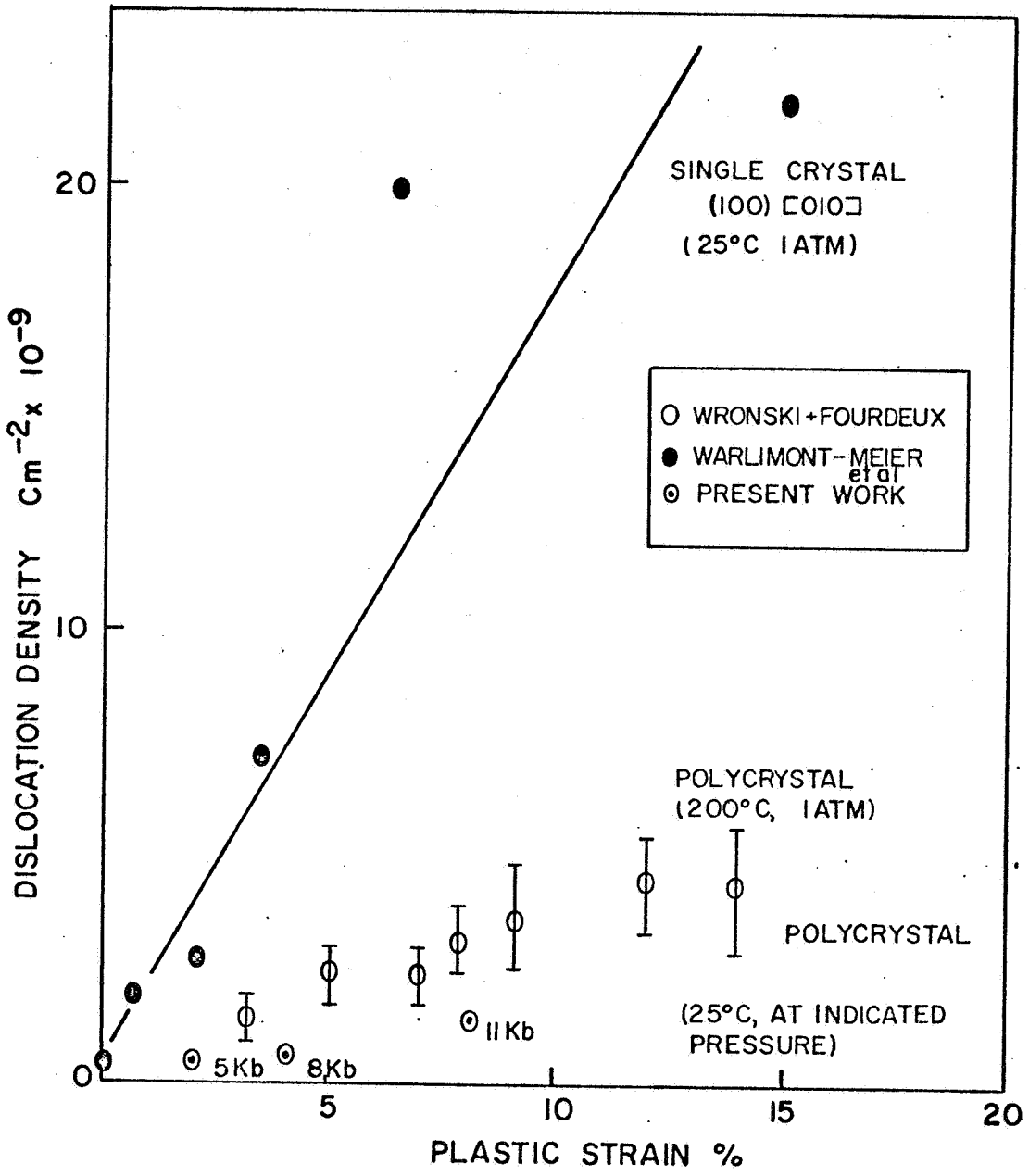

Fig. 9 Dislocation density in recrystallized PM tungsten as a function of strain to fracture at indicated pressures. The curve compares the data with that for high purity (mono and polycrystalline) tungsten deformed in tension under ambient conditions.

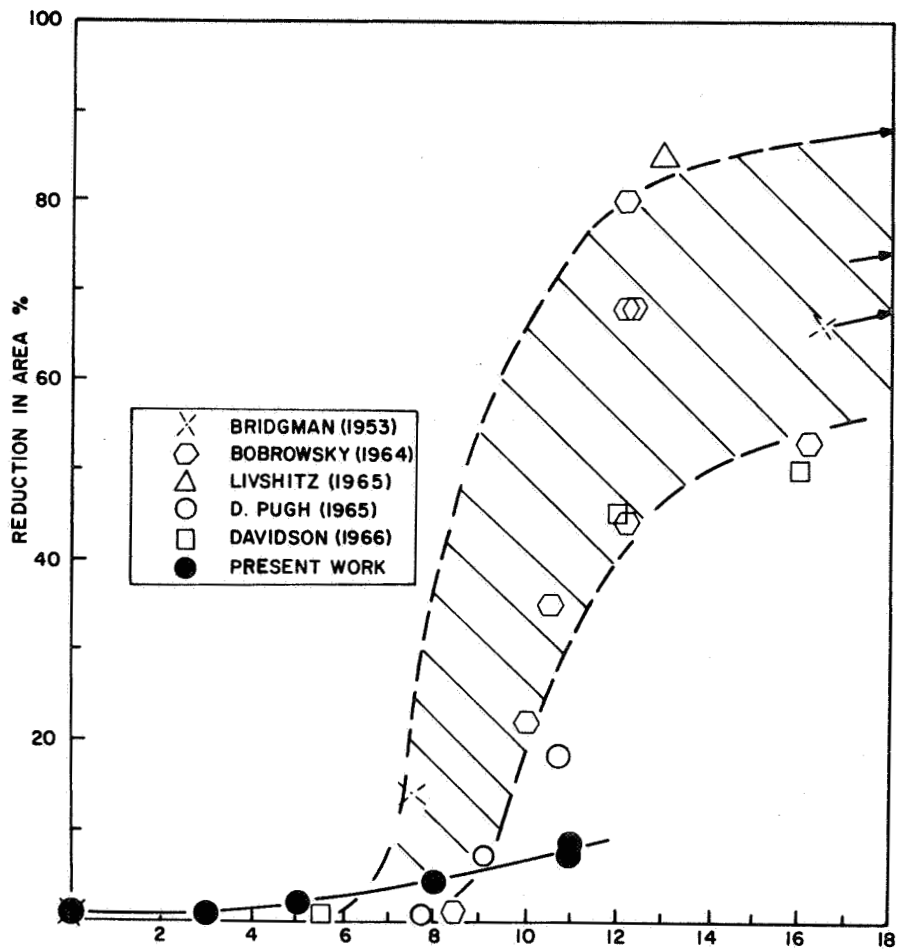

Fig. 10. Pressure dependence of the ductility (reduction in area) of recrystallized PM tungsten. Data reported previously for tungsten is collated in the figure and their range of values indicated by the band.

Fig. 11. Electron fractograph showing intergranular and transgranular fracture in recrystallized PM tungsten strained to fracture at 8 kilobars.

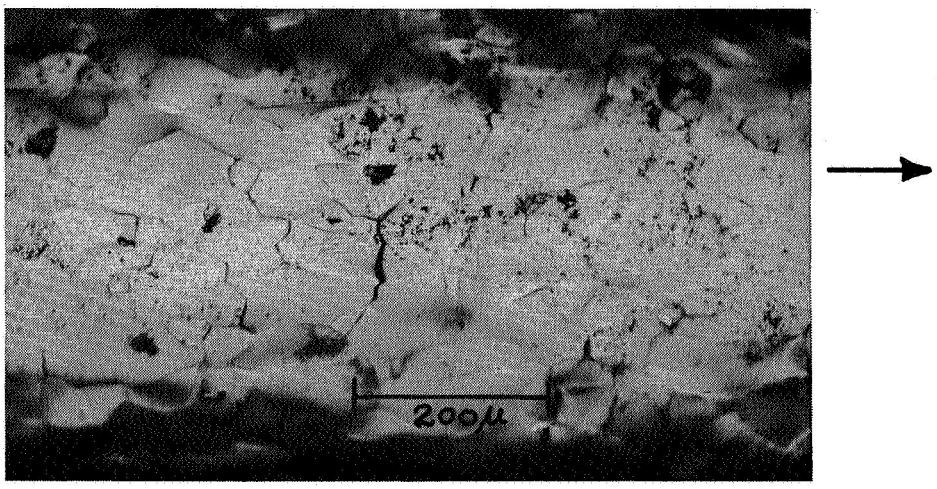

(a)

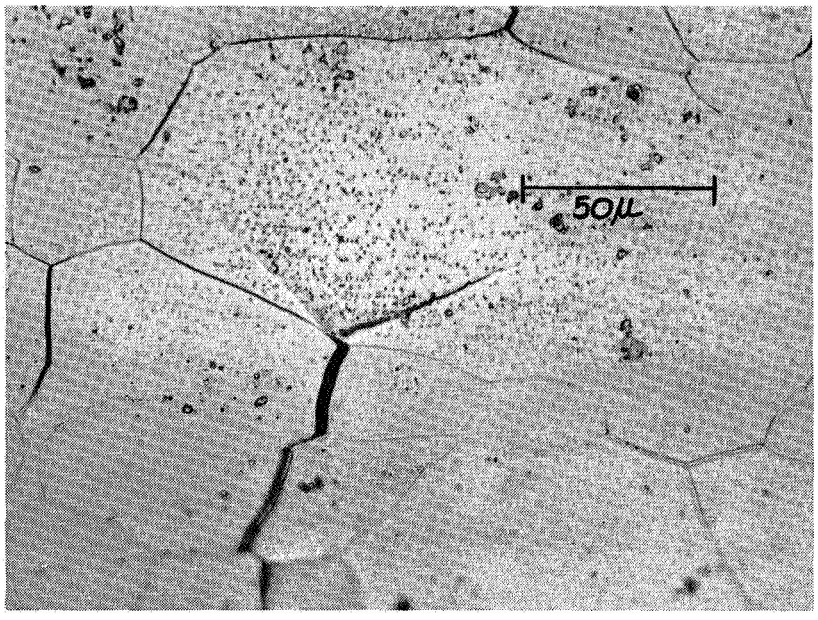

(b)

Fig. 12. Optical micrographs showing intergranular and transgranular cracks: (a) along the complete gage length; (b) a transgranular crack associated with an intergranular crack. Recrystallized PM tungsten strained to fracture at 11 kilobars. The arrow shows the tensile axis.

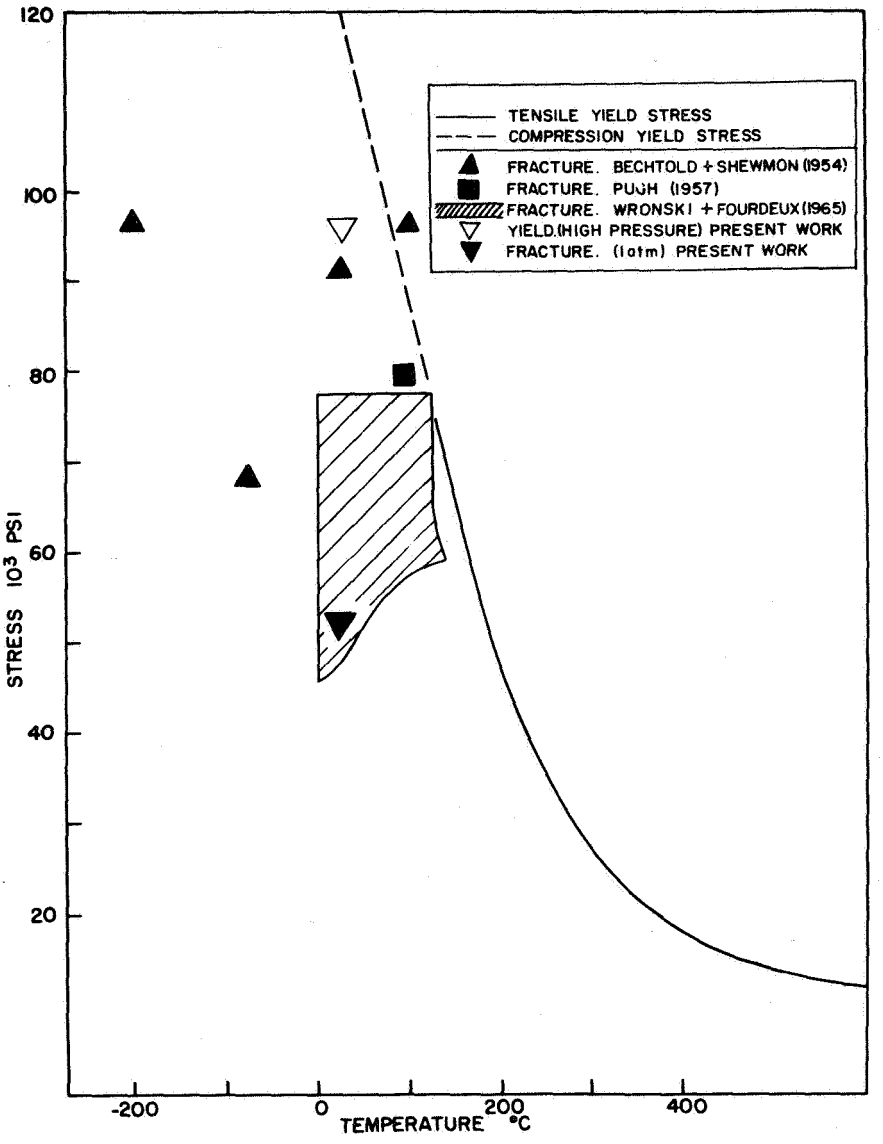

Fig. 13. Comparison of yield stress at high pressure with yield and fracture stresses reported for atmospheric pressure.

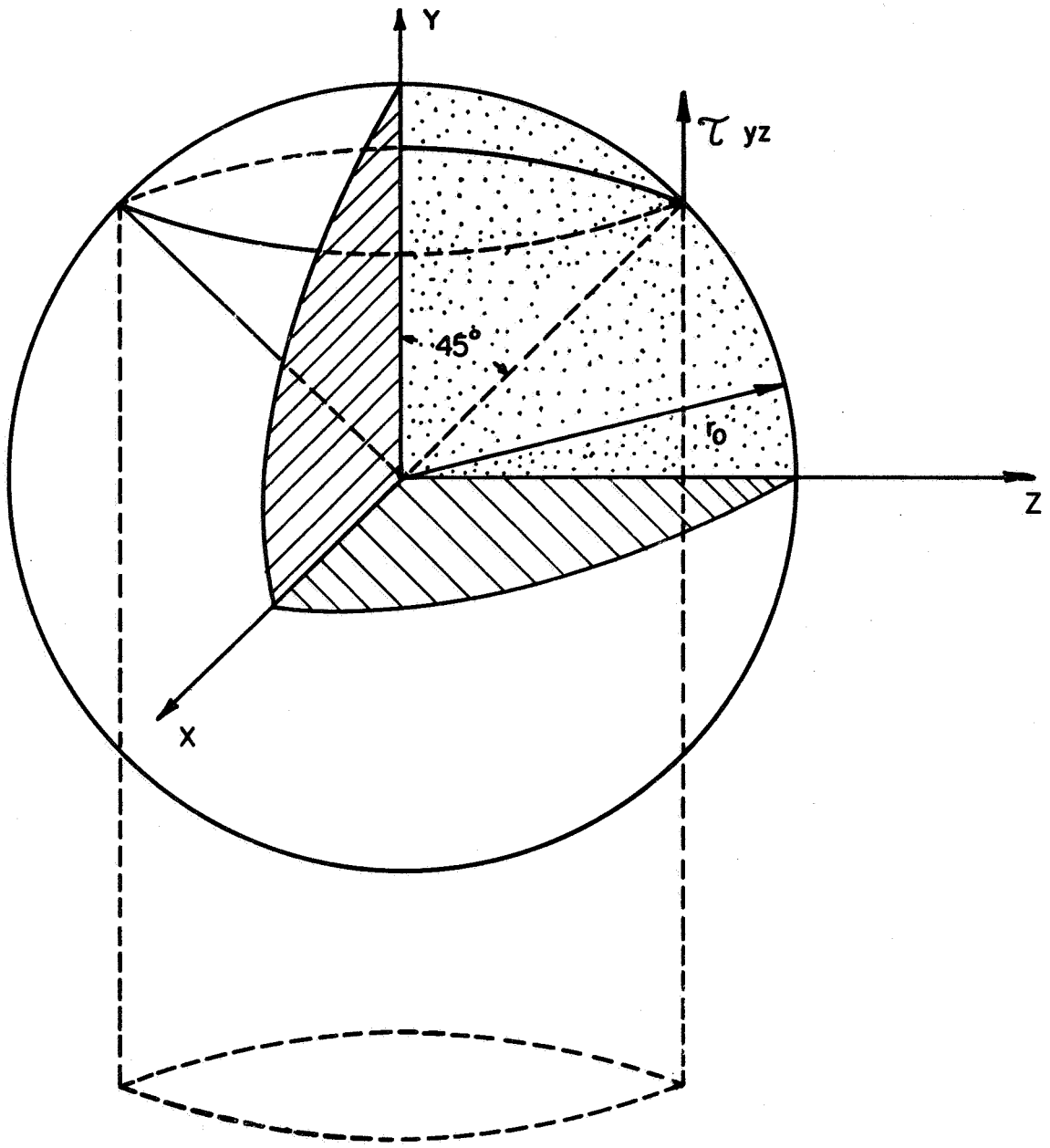

Fig. 14. Shear stress at the interface of a spherical inclusion of radius r_o.

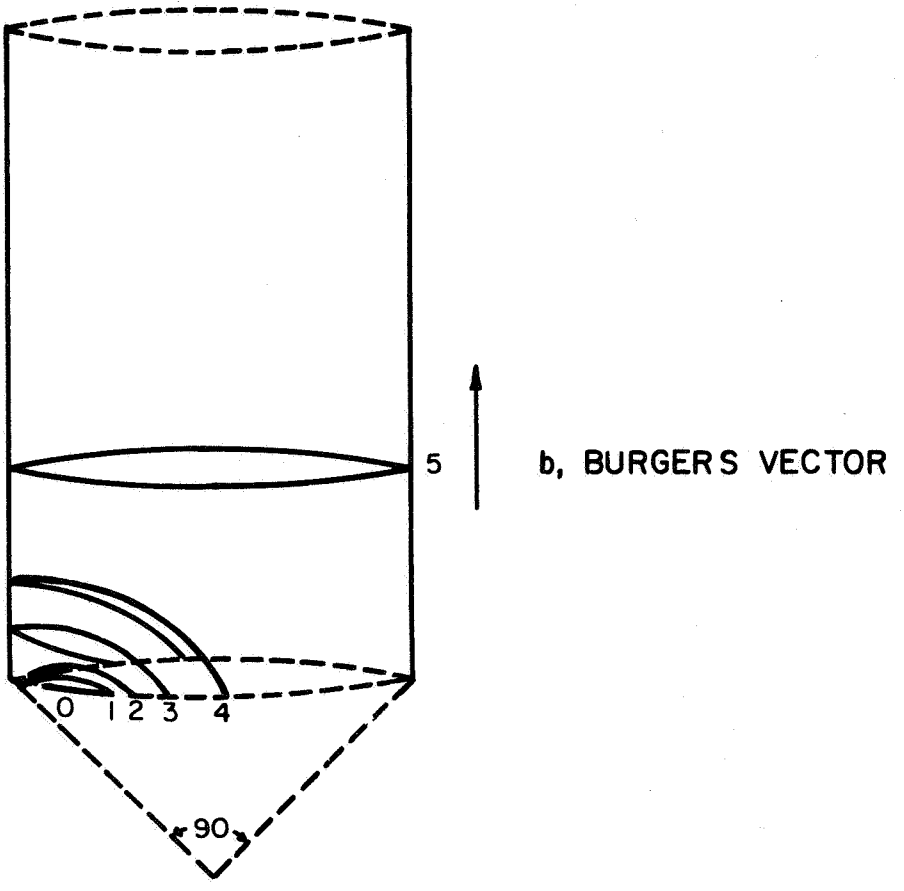

Fig. 15. The states of formation of a perfect prismatic loop by pure glide.

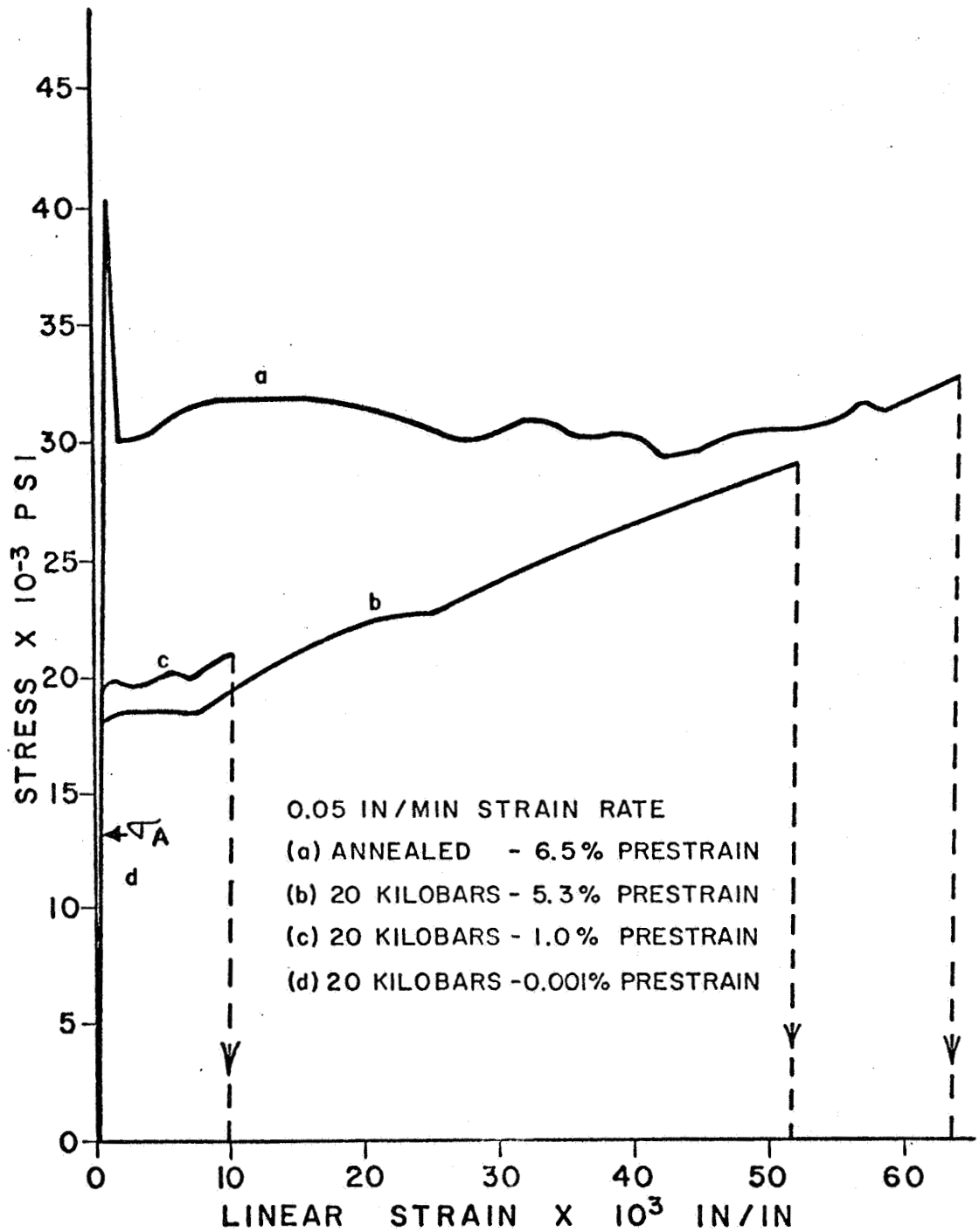

Figure 16 Tensile prestraining 0.09 wt%C alloy subsequent to 20 kilobars pressurization.

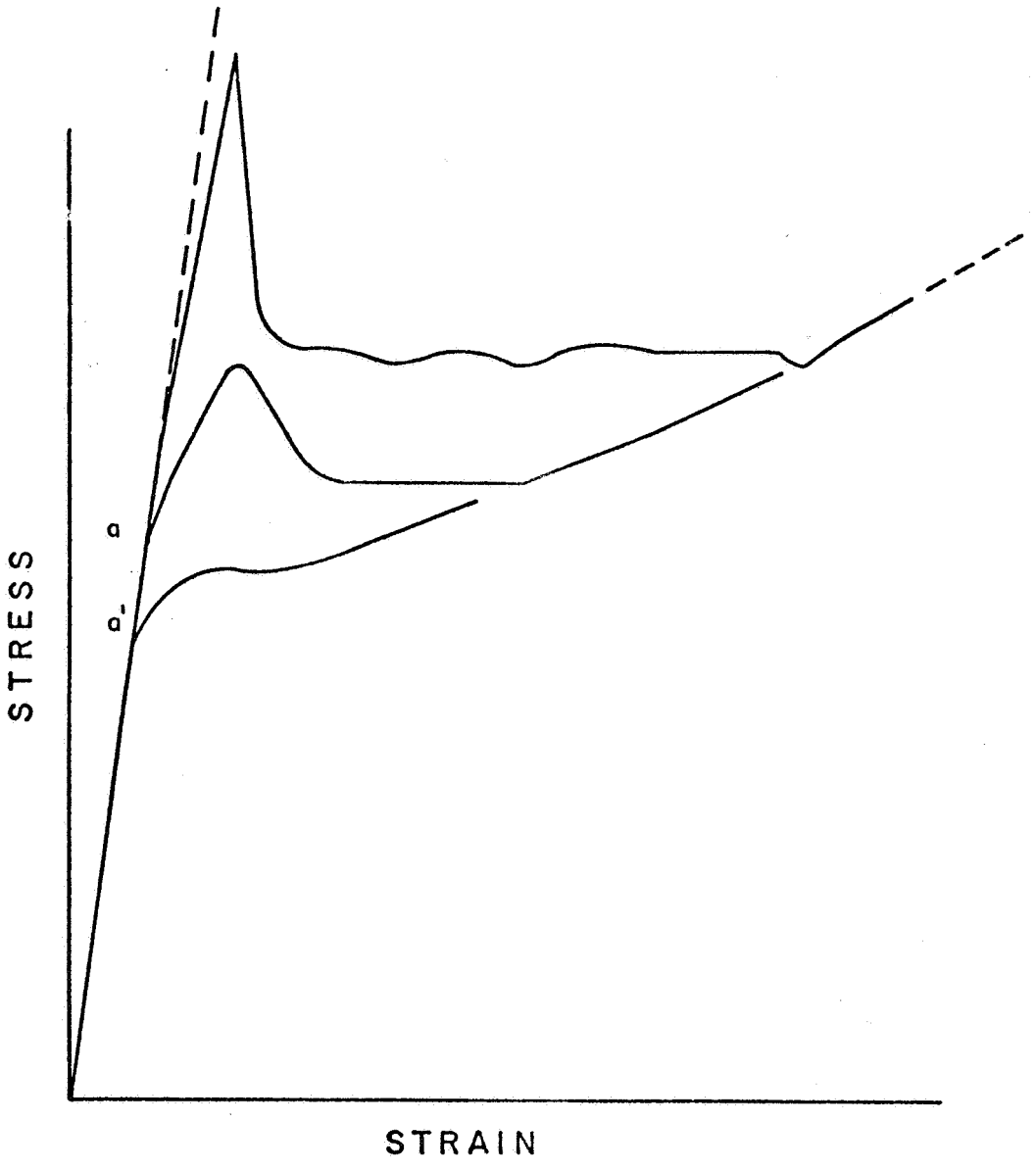

Figure 17 Schematic tensile stress-strain curves demonstrating the characteristic featural changes in yield behavior for iron-carbon alloys with increasing pressurization.

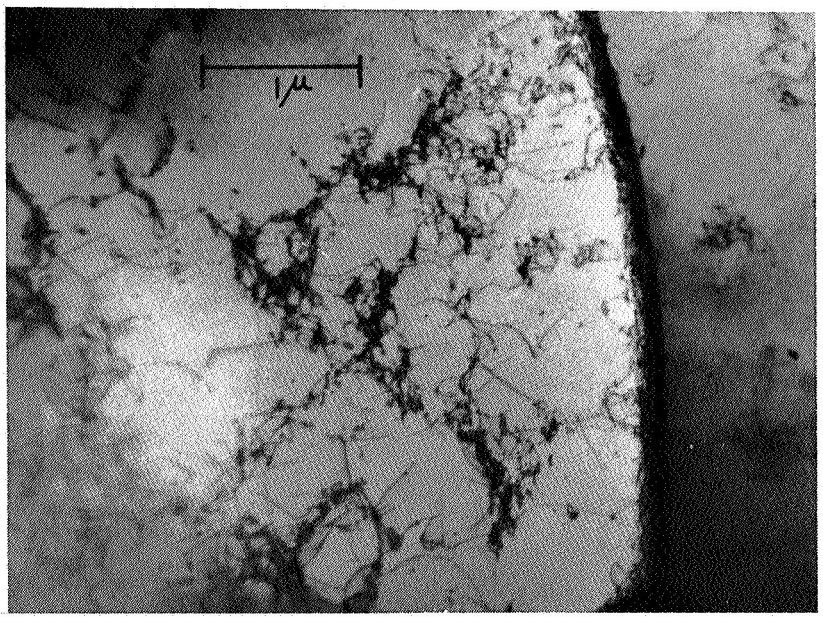

(a)

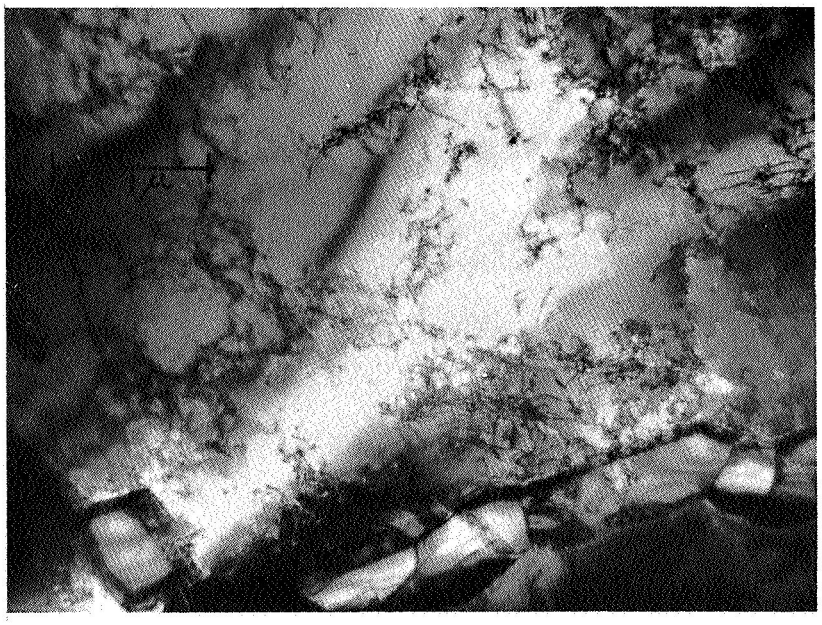

(b)

Fig. 18. Illustration of dislocation distribution in 0.09 wt%C alloy after subjection to 20 kilobars and subsequent tensile prestraining to microyield point $\bar{\sigma}_A$.

(a) variations in dislocation density within grains, X20,000;

(b) tangles near carbide particles.

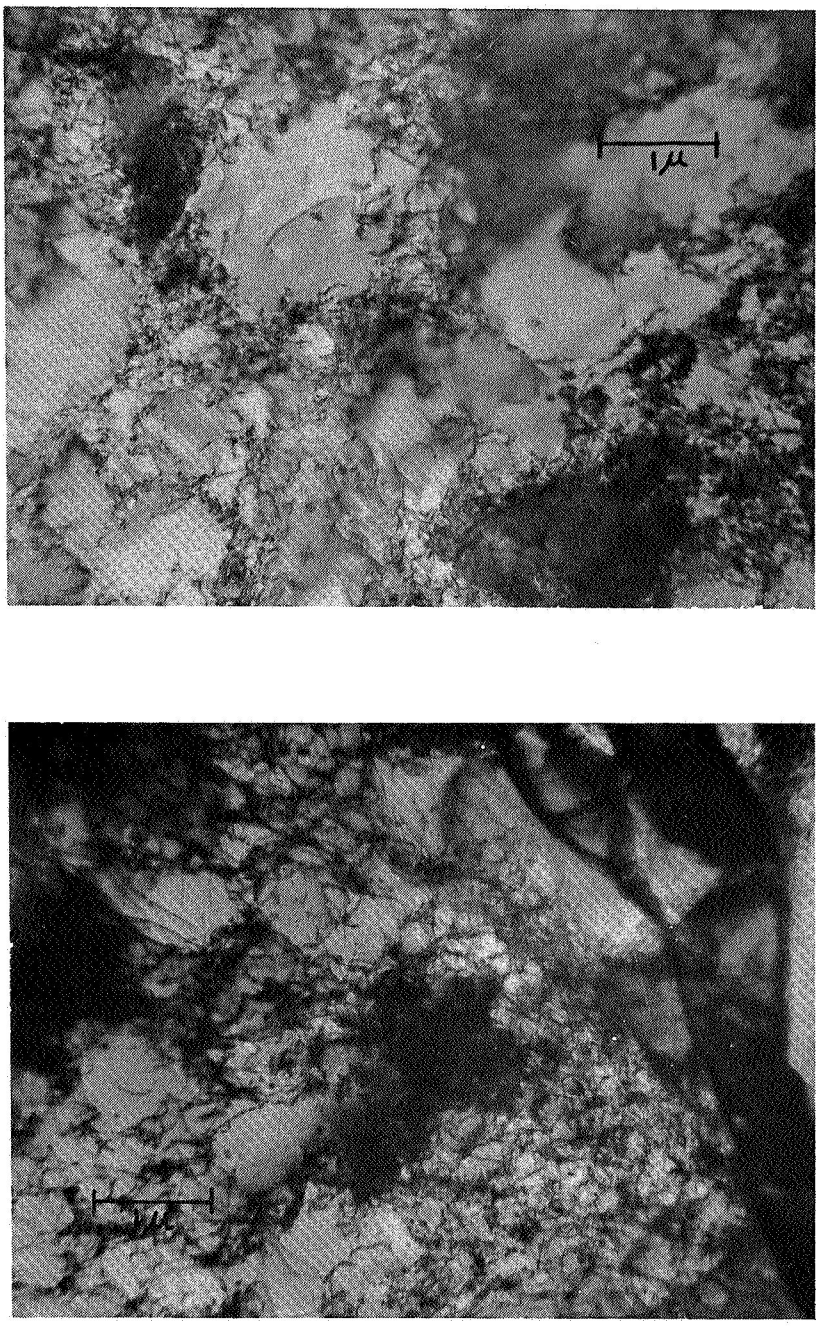

Fig. 19. Examples of dislocation clusters and cell structure developed in annealed 0.09 wt.%C alloy on tensile prestraining 6.5%. X15,000.

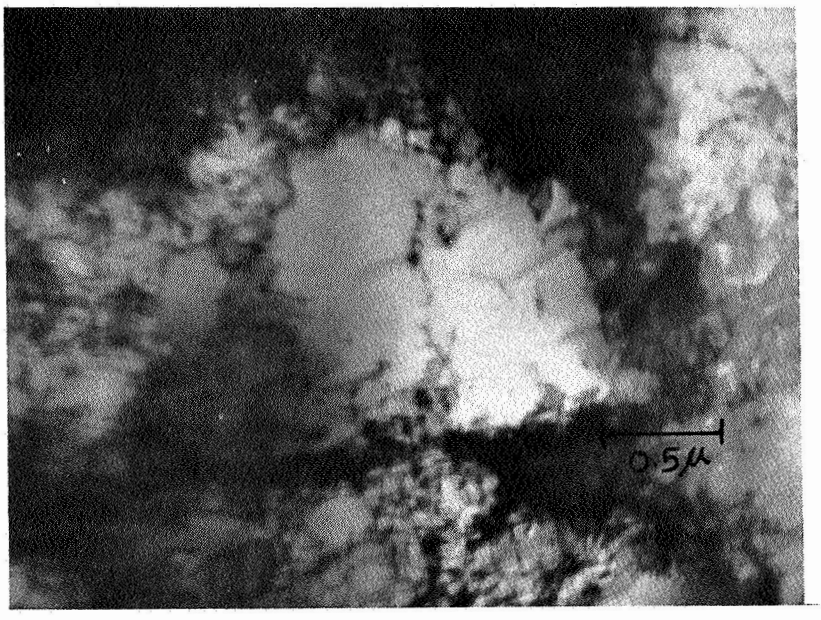

(a)

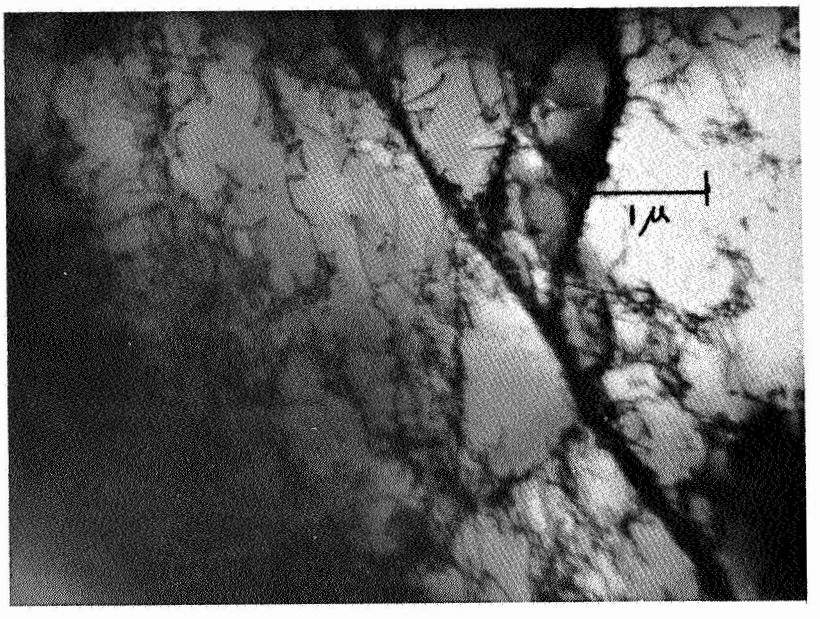

(b)

Fig. 20. Dislocation clusters (cell structure) in 0.09 wt.%C alloy subjected to 20 kilobars and subsequently tensile prestrained 5.3%; (a) X30,000, (b) X15,000.